IEEE Access
Multidisciplinary | Rapid Review | Open Access Journal

Received September 21, 2018, accepted October 29, 2018, date of publication November 9, 2018,
date of current version December 18, 2018.

Digital Object Identifier 10.1109/ACCESS.2018.2879649

Robust Controller Design for Non-Minimum Phase UAV System and System Analysis

JIA-HORNG YANG, (Member, IEEE), AND HUA-KAI XU
Department of Electrical and Electronic Engineering, Chung Cheng Institute of Technology, National Defense University, Taoyuan 33551, Taiwan
Corresponding author: Jia-Horng Yang (yang.jiahorng@gmail.com)

This was supported by the Ministry of Science and Technology, MOST of under Grant MOST 107-2221-E-606-013.

ABSTRACT Different from other references that use Ziegler–Nichols method or another trial and error method to design the proportional–integral–derivative (PID) controller, this paper is based on the precise controller design in combination with the root locus criterion. According to the system properties and the task requirements, we applied the model reduction method, root locus criterion, root contour, pole-zero placement, frequency response, and orthodox PID criterion to design various controllers. Besides, we analyzed the system responses in a time domain to obtain the optimal controller parameters. We also designed a robust controller to give the system better relative stability through the comparisons of system performances in the frequency domain. Furthermore, in this paper, we also created the reverse gain PID controller to deal with the negative effects of the non-minimum phase system. Not only does this controller improve both the transient response and steady-state error but also enhance the relative stability of the system at the same time. Finally, according to the system properties, this paper can make the controllability of UAV much better by a variety of design methods and flexible controller applications, and then expand the application fields and scopes of UAVs. In sum, the research content is academic, practical, and very efficient as it can be used as reference material that can be applied in further follow-up research.

INDEX TERMS Ziegler-Nichols method, root locus, root contour, PID, controller design, non-minimum phase system.

I. INTRODUCTION

The marked development of industrial technology and the rapid growth in the processing speed of computer chips have coincided with the rise of humanitarianism. Unmanned Aerial Vehicle (UAV), whether its use in the military or private technology, has become more and more advanced, Research on UAV has become an increasingly popular topic of studies, and such studies have received more and more investment so as to expand the uses of UAV, e.g., military use, environmental exploration, landscape filming, cross-border transportation, disaster relief, and so on. In recent years, the research and use of this technology have progressed significantly. However, UAV applications have many limiting conditions caused by the uncertainties while flying (e.g., air density, temperature difference, airflow disturbance, compressive strength of carrier and sensor). These factors inhibit the developments and applications of UAV.

In consideration of the difficulties of the operating environment, it is difficult to overcome the negative impact of non-minimum phase systems on drone flight stability. In this paper, we propose to extend the UAV's application through various controller designs. These designs, which based on the criterions of the Root Locus (RL) and root contour (RC), work to effectively improve both the transient response and steady-state error performance of the UAV system. In addition, in this paper we created a new controller called "Reverse Gain PID Controller" to help find the appropriate controller parameters more quickly and solve the negative effects of the non-minimum phase system to obtain better performance in the system. The above is the main motivation in the research done in this paper.

UAV have many limitations in their applications, because there are too many uncertainties in the flight environment, such as air flow disturbances, air density, temperature difference, etc. In addition, the lack of real hardware in UAV also worsens the performance of UAV system, such as the defect of the sensor's resistance to pressure and cold, the high fuel consumption and insufficient thrust of the vehicle, and the shortage of controller design techniques for UAV motion, etc. All of the above-mentioned current situations are restraining the application and development of the flying vehicles. In the sight of this, this research proposes a variety of methods based

on the root contour theory to design the controller, which can effectively improve the response of the UAV system for the UAV's complex, distressed operating environment and different system characteristics, and also raise the relative stability of the system and extend the application range of UAV. Besides, some UAV have the negative effects of non-minimum phase system. Although some good control methods can indeed improve the response of nonlinear or non-minimum phase systems [1]–[8]. However, the methods currently being solved are too complex and have limited effectiveness. In the sight of the difficulty in improving non-minimum phase systems, this study also responded to the obstacle by creating a new "Reverse Gain PID Controller."

The summary of research contributions is as the following 5 key points:

1) According to the characteristics of 12 different UAV systems, a variety of controllers have been designed. Therefore, the adopted design would be from the paper which has the most extensive analysis for the controller designs of UAV motions. The content of the paper is rich and highly applicable and can be used by relevant researchers.
2) The controllers of this research not only improve the system responses of UAVs in time domain, but also emphasize the response analysis in frequency domain and the designs of the robust controller. Therefore, the designed controllers can give the systems better relative stabilities that can increase the UAVs' survival rate when operating in unknown environments.
3) In the face of the unstable non-minimum phase system, this study proposes "Reverse Gain PID Controller" to deal with it. In addition to effectively improving the system response, "Reverse Gain PID Controller" also ameliorates the relative stability of the system at the same time.
4) The "Reverse Gain PID Controller" is easier to implement than other methods that can improve non-minimum phase systems, and it is not as complicated in operation as other methods. Besides, it has a better improvement in terms of the coupling effect between the inverse response and the settling time of the non-minimum phase systems.
5) The root contour theory was applied in the controller design process, which has a higher degree of accuracy and effectiveness in the selection of the multi-parameters of the controllers.

In addition, to improve the system behavior, the designing methods of this research not only extend the applications of UAV but can also be used as reference material or be applied in follow up research.

II. UAV STRUCTURE

A. UAV SELECTION

In this paper, the scale model of the Cessna 182 is selected as the experimental UAV, and we call this selected UAV "scale Cessna 182" by making its clear definition in order to distinguish it from the prototype Cessna 182. The ratio of the scale Cessna 182 to the prototype Cessna 182 is 1: 6.65.

Cessna series are manufactured in Wichita, Kansas, USA, and they are widely used by the US Air Force for education and training purposes. Because the performance of the scale machine is similar to the prototype, the scale model is often used to carry out relevant experiments using the real flight equipment. The scale Cessna 182 is shown in FIGURE 1 [9], and the structure of the body can be seen in FIGURE 2 [10]. The geometric parameters of the scale Cessna 182 are also shown in FIGURE 3 [11] and Table 1 [12].

At present, the research of UAVs is divided into two types. The first category is the application research of UAV. For example, after UAVs are loaded with different payloads to collect information, subsequent data processing is performed with UAVs equipped with camera devices or sensors, image

FIGURE 1. Scale Cessna 182 – 1/6.65 ratio to the Prototype Cessna 182 [9].

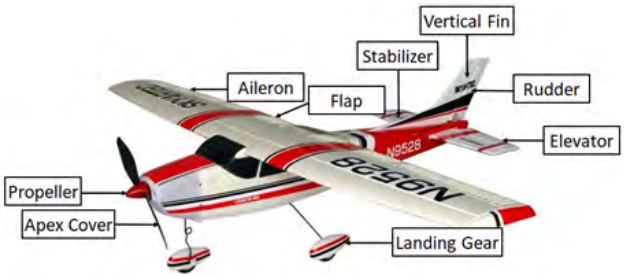

FIGURE 2. Structure of Scale Cessna 182 [10], [11].

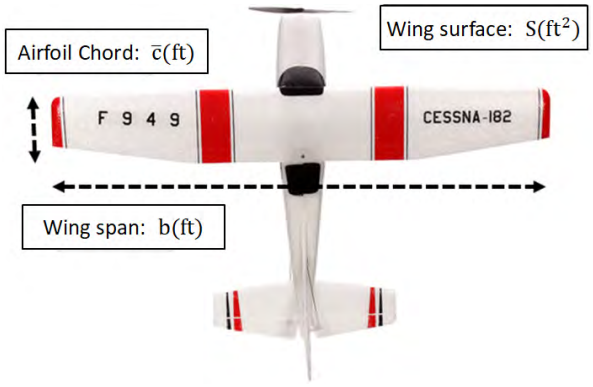

FIGURE 3. Geometry parameter definition of Scale Cessna 182 [12].

TABLE 1. Units for magnetic properties.

UAV Part	Scale factor (SF = 6.65)
Wing span (ft) b	5.4135
Wing surface (ft^2) S	3.9346
True airspeed (ft/sec) V_{P_1}	85.3511
Dynamic pressure (lbs/ft^2) $\bar{q}_1=\frac{1}{2}\rho V_{P_1}{}^2$	7.4586
Steady state angle of attack (deg) α	0

detection and environmental exploration work; the second type of research is UAV motion analysis, improvement or controller design. This paper belongs to the second type of research.

In the second type of UAV movement research, most of the literature only focuses on the sub-systems of UAVs, especially the more easily analyzed longitudinal movements, but there is a lack of interest in the controller design for more complex lateral motions. However, when the UAV is in flight, its flight stability is affected by both the state of motion of the longitudinal motion and the lateral motion. At the same time, instability of any subsystem in the longitudinal motion and the lateral motion will harm the flight safety of the UAV. However, as far as we know, apart from C.-Y. Yang's master thesis [12], none of the journals have conducted a comprehensive discussion on the subsystems of the UAV and improved the design of the controller. Therefore, this is also why C. -Y. Yang's research results will be used as the main reference for comparison. In addition to studying all the systems of longitudinal motion and lateral motion of UAV, we also designed a variety of controllers for 12 different systems and improved the design of the non-minimum phase system that could not be overcome in C.-Y. Yang's thesis, and successfully developed the ''Reverse Gain PID Controller''. Therefore, this paper is currently the most comprehensive one in the study of controller design for UAV motion.

B. MODEL ESTABLISHMENT OF THE UAV

The basic dynamic motion of the aircraft has six different degrees in terms of freedom, that is, the horizontal movement and the rotation around the X, Y, and Z axes, respectively (shown in FIGURE 4 [13]), which can be used to analyze the longitudinal and horizontal motions of the UAV movement. In this research, the experimental UAV, scale Cessna 182, has the scale ratio of 1: 6.65 of the prototype Cessna 182, and it has similar system performances to the prototype aircraft. In addition, because the basic dynamics and the derivation process of the aircraft model are of general knowledge, this paper only gives a brief description on how to derive the formula process of the UAV model and highlights the system analysis and design of various controllers. The detailed information for the derivation process of the UAV mathematical model can be referred in [14] or can be easily found on the internet.

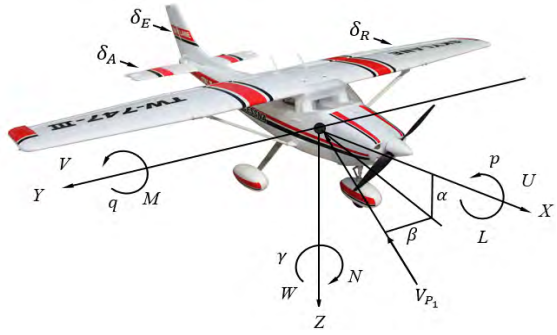

FIGURE 4. Six degrees of freedom for aircraft [13].

C. THE LONGITUDINAL MOTION EQUATIONS OF SCALE CESSNA 182

The following is a brief derivation and description of the longitudinal motion equation for aircraft. Again, the complete derivation of aircraft motion's equation can be referred in reference [14]. In FIGURE 4, as we know, the longitudinal linearization equation of the aircraft can also be represented by equation (1).

$$\begin{aligned}
\dot{u} &= -g\cos\Theta_1\theta + \left(X_u + X_{T_u}\right)u + X_\alpha\alpha + X_{\delta_E}\delta_E \\
V_{P_1}\dot{\alpha} &= -g\sin\Theta C\, Z_u u + Z_{\dot{\alpha}}\dot{\alpha} + Z_\alpha\alpha + \left(Z_q + V_{P_1}\right)\dot{\theta} \\
&\quad + Z_{\delta_E}\delta_E \\
\ddot{\theta} &= \left(M_u + M_{T_u}\right)u + \left(M_\alpha + M_{T_\alpha}\right)\alpha \\
&\quad + M_{\dot{\alpha}}\dot{\alpha} + M_q\dot{\theta} + M_{\delta_E}\delta_E
\end{aligned} \tag{1}$$

Where $\dot{u}$ is the derivative of the forward speed U, and $\dot{\alpha}$ is the derivative of the angle of attack (AOA), α. Besides, $\dot{\theta}$ and $\ddot{\theta}$ are the first and second derivative of the pitch angle θ, respectively. Θ_1 is the pitch angle in the steady state. Besides, the other parameter values are also shown in Table 2 [14]–[16], Table 3 [15], [16], and the FIGURE 4.

Using the Laplace transformation to equation (1) and assuming the initial conditions are zero, the initial position of the system being balanced, we can get the result as follows:

$$\begin{aligned}
\mathcal{L}(\delta_E) &= \delta_E(s) \\
\mathcal{L}(u) &= \mathrm{u}(s); \quad \mathcal{L}(\dot{u}) = su(s) \\
\mathcal{L}(\alpha) &= \alpha(s); \quad \mathcal{L}(\dot{\alpha}) = s\alpha(s) \\
\mathcal{L}(\alpha) &= \theta(s); \quad \mathcal{L}(\dot{\theta}) = s\theta(s);\ \mathcal{L}(\ddot{\theta}) = s^2\theta(s)
\end{aligned}$$

When you substitute the above transformation results in Eq. (1), we can get Eq. (2):

$$\begin{aligned}
&\left(s - \left(X_u + X_{T_u}\right)\right)\mathrm{u}(s) - X_\alpha\alpha(s) + X_\alpha\alpha(s) + g\cos\Theta 1(s) \\
&= X_{\delta_E}\delta_E(s) \\
&-Z_u u(s) + \left(s\left(V_{P_1} - Z_{\dot{\alpha}}\right) - Z_\alpha\right)\alpha(s) \\
&\quad + \left(-s\left(Z_q + V_{P_1}\right) + g\sin\Theta_1\right)\theta(s) \\
&= Z_{\delta_E}\delta_E - \left(M_u + M_{T_u}\right) \\
&u(s) - \left(M_{\dot{\alpha}}s + \left(M_\alpha + M_{T_\alpha}\right)\right)\alpha(s) + s(s - M_q)\theta(s) \\
&= M_{\delta_E}\delta_E
\end{aligned} \tag{2}$$

TABLE 2. The symbols of aircraft motion with six degree of freedom [14]–[16].

Parameter	Quantity
U	Forward speed
V	Slipping speed
θ	Pitch angle
α	Angle of attack (AOA)
W	Vertical speed
β	Angle of side slip (Sideslip angle)
p	Angular velocity of X axis
□	Roll angle
q	Angular velocity of Y axis
ψ	Yaw angle
r	Angular velocity of Z axis
δ_E	Angle of elevator
L	Moment of X axis
δ_A	Angle of aileron
M	Moment of Y axis
δ_R	Angle of rudder
N	Moment of Z axis
V_{P_1}	Indicated air speed
Θ_1	Pitch angle in the steady state
g	Gravity
$I_1 = \frac{I_{XZ}}{I_{XX}}$	Moment of inertia: I_1
$I_2 = \frac{I_{XZ}}{I_{ZZ}}$	Moment of inertia: I_2
SF	Scale factor: the ratio between UAV and real aircraft

TABLE 3. Relationships for partial derivatives of longitudinal aerodynamics [15], [16].

	Partial derivative of forward force	Partial derivative of normal force	Partial derivative of pitching moment M
Advance speed (u)	X_u	Z_u	M_u
Angle of attack (α), AOA	X_α	Z_α	M_α
Angle of elevator (δ_E)	X_{δ_E}	Z_{δ_E}	M_{δ_E}
Vertical speed (w)	X_w	Z_w	M_w
Pitch rate (q)		Z_q	M_q
Change rate of vertical velocity ($\dot{w}$)			$M_{\dot{w}}$
Rate of AOA ($\dot{\alpha}$)		$Z_{\dot{\alpha}}$	$M_{\dot{\alpha}}$
Thrust of engine to speed (T_u)	X_{T_u}		M_{T_u}
Thrust of engine to AOA (T_α)			M_{T_α}

Now, let the angle of the elevator, $\delta_E(t)$, be the system input, and the output variables of X, Y, and Z axes are $u(t)$, $\alpha(t)$, and $\theta(t)$, respectively. So we can define the three transfer functions as $\left\{\frac{u(s)}{\delta_E(s)}, \frac{\alpha(s)}{\delta_E(s)}, \frac{\theta(s)}{\delta_E(s)}\right\}$ for prototype Cessna 182.

TABLE 4. The ratios of longitudinal aerodynamics for Scale Cessna 182 [12].

Parameter	Scale factor SF=6.65
X_u/X_{u_S}	$\sqrt{SF}$
X_δ/X_{δ_S}	1
Z_u/Z_{u_S}	$\sqrt{SF}$
Z_δ/Z_{δ_S}	1
M_u/M_{u_S}	$SF\sqrt{SF}$
M_δ/M_{δ_S}	SF
X_α/X_{α_S}	1
M_q/M_{q_S}	$\sqrt{SF}$
Z_α/Z_{α_S}	1
Z_q/Z_{q_S}	$\sqrt{SF}/SF$
M_α/M_{α_S}	SF
$M_{\dot{w}}/M_{\dot{w}_S}$	SF
X_w/X_{w_S}	$\sqrt{SF}$
$Z_{\dot{\alpha}}/Z_{\dot{\alpha}_S}$	$\sqrt{SF}/SF$
Z_w/Z_{w_S}	$\sqrt{SF}$
$M_{\dot{\alpha}}/M_{\dot{\alpha}_S}$	$SF\sqrt{\frac{1}{SF}}$
M_w/M_{w_S}	$SF\sqrt{SF}$
$X_{T_u}/X_{T_{u_S}}$	$\sqrt{SF}$
$M_{T_u}/M_{T_{u_S}}$	$SF\sqrt{SF}$
$M_{T_\alpha}/M_{T_{\alpha_S}}$	SF

After reintegrating Eq. (2), we can get Eq. (3), as shown at the bottom of this page, [12].

Using Cramer theory to solve Eq. (3), we can get the transfer functions as Eqs. (4)–(6), as shown at the top of the next page.

In addition, before proceeding with the system analysis and controller design for the UAV (scale Cessna 182), the ratios of the aerodynamic parameters and geometric parameters between the scale Cessna 182 and prototype Cessna 182 must be considered. The ratio result is shown in Table 4 [12]. Since the ratio of scale Cessna 182 to prototype Cessna 182 is 1: 6.65, we can set the scale factor, SF, as the value of 6.65. Besides, we can also obtain the partial derivative of longitudinal aerodynamics as Table 5 [12]. And after reintegrating and deriving Eq. (2) with the parameters in Table 5, we can obtain the three transfer functions of the scale Cessna 182 shown in Eq. (7-9), as shown at the top of the next page, [12].

Therefore, we can get the transfer function from the elevator angle ($\delta_{E_s}(s)$) to the AOA ($\alpha_s(s)$) of the Scale Cessna 182 as Eq. (7):

And the transfer function from the elevator angle $\delta_{E_s}(s)$ to the speed ($u_s(s)$) of the Scale Cessna 182 as Eq. (8):

$$\begin{bmatrix} (s-(X_u+X_{T_u})) & -X\alpha & g\cos\Theta 1 \\ -Z_u & (s(V_{P_1}-Z_{\dot{\alpha}})-Z_\alpha & (-s(Z_q+V_{P_1})+g\sin\Theta 1) \\ -(M_u+M_{T_u}) & -(M_{\dot{\alpha}}s+(M_\alpha+M_{T_\alpha}) & s(s-M_q) \end{bmatrix} \begin{Bmatrix} \frac{u(s)}{\delta_E(s)} \\ \frac{\alpha(s)}{\delta_E(s)} \\ \frac{\theta(s)}{\delta_E(s)} \end{Bmatrix} = \begin{Bmatrix} X_{\delta_E} \\ Z_{\delta_E} \\ M_{\delta_E} \end{Bmatrix} \quad (3)$$

$$\frac{u(s)}{\delta_E(s)} = \frac{\begin{vmatrix} X_{\delta_E} & -X\alpha & g\cos\Theta 1 \\ Z_{\delta_E} & (s(V_{P_1} - Z_{\dot{\alpha}}) - Z_\alpha & (-s(Z_q + V_{P_1}) + g\sin\Theta 1) \\ M_{\delta_E} & -(M_{\dot{\alpha}}s + (M_\alpha + M_{T_\alpha}) & s(s - M_q) \end{vmatrix}}{\begin{vmatrix} (s - (X_u + X_{T_u})) & -X\alpha & g\cos\Theta 1 \\ -Z_u & (s(V_{P_1} - Z_{\dot{\alpha}}) - Z_\alpha & (-s(Z_q + V_{P_1}) + g\sin\Theta 1) \\ -(M_u + M_{T_u}) & -(M_{\dot{\alpha}}s + (M_\alpha + M_{T_\alpha}) & s(s - M_q) \end{vmatrix}} \tag{4}$$

$$\frac{\alpha(s)}{\delta_E(s)} = \frac{\begin{vmatrix} (s - (X_u + X_{T_u})) & X_{\delta_E} & g\cos\Theta 1 \\ -Z_u & Z_{\delta_E} & (-s(Z_q + V_{P_1}) + g\sin\Theta 1) \\ -(M_u + M_{T_u}) & M_{\delta_E} & s(s - M_q) \end{vmatrix}}{\begin{vmatrix} (s - (X_u + X_{T_u})) & -X\alpha & g\cos\Theta 1 \\ -Z_u & (s(V_{P_1} - Z_{\dot{\alpha}}) - Z_\alpha & (-s(Z_q + V_{P_1}) + g\sin\Theta 1) \\ -(M_u + M_{T_u}) & -(M_{\dot{\alpha}}s + (M_\alpha + M_{T_\alpha}) & s(s - M_q) \end{vmatrix}} \tag{5}$$

$$\frac{\theta(s)}{\delta_E(s)} = \frac{\begin{vmatrix} (s - (X_u + X_{T_u})) & -X\alpha & X_{\delta_E} \\ -Z_u & (s(V_{P_1} - Z_{\dot{\alpha}}) - Z_\alpha & Z_{\delta_E} \\ -(M_u + M_{T_u}) & -(M_{\dot{\alpha}}s + (M_\alpha + M_{T_\alpha}) & M_{\delta_E} \end{vmatrix}}{\begin{vmatrix} (s - (X_u + X_{T_u})) & -X\alpha & g\cos\Theta 1 \\ -Z_u & (s(V_{P_1} - Z_{\dot{\alpha}}) - Z_\alpha & (-s(Z_q + V_{P_1}) + g\sin\Theta 1) \\ -(M_u + M_{T_u}) & -(M_{\dot{\alpha}}s + (M_\alpha + M_{T_\alpha}) & s(s - M_q) \end{vmatrix}} \tag{6}$$

$$\frac{\alpha_s(s)}{\delta_{E_s}(s)} = \frac{-44.985s^3 - 20103s^2 - 2363.5s + 1730.9}{86.1189s^4 + 1985.9478s^3 + 16150s^2 + 2082.5s + 945.7337} \tag{7}$$

$$\frac{u_s(s)}{\delta_{E_s}(s)} = \frac{-875.3631s^2 - 195940s + 1012100}{86.1189s^4 + 1985.9478s^3 + 16150s^2 + 2082.5s + 945.7337} \tag{8}$$

$$\frac{\theta_s(s)}{\delta_{E_s}(s)} = \frac{-19893s^2 - 105510s - 15567}{86.1189s^4 + 1985.9478s^3 + 16150s^2 + 2082.5s + 945.7337} \tag{9}$$

The transfer function from the elevator angle ($\delta_{E_s}(s)$) to the pitch angle ($\theta_s(s)$) of the Scale Cessna 182 as Eq. (9):

D. EQUATIONS OF LATERAL MOTION

The linearized equation of lateral motion for scale Cessna 182 after deriving can be seen in Eq. (10) [14]:

$$\begin{aligned} &(V_{P_1}\dot{\beta} + V_{P_1}\dot{\psi}) \\ &\quad = g\phi + Y_\beta\beta + Y_{\dot{\phi}}\dot{\phi} + Y_{\dot{\psi}}\dot{\psi} + Y_{\delta_A}\delta_A + Y_{\delta_R}\delta_R \\ &\ddot{\phi} - \frac{I_{XZ}}{I_{XX}}\ddot{\psi} = L_\beta\beta + L_{\dot{\phi}}\dot{\phi} + L_{\dot{\psi}}\dot{\psi} + L_{\delta_A}\delta_A + L_{\delta_R}\delta_R \\ &\ddot{\psi} - \frac{I_{XZ}}{I_{ZZ}}\ddot{\phi} = N_\beta\beta + N_{\dot{\phi}}\dot{\phi} + N_{\dot{\psi}}\dot{\psi} + N_{\delta_A}\delta_A + N_{\delta_R}\delta_R \end{aligned} \tag{10}$$

Where $\dot{\beta}$ is the differential of sideslip angle, β. $\dot{\Psi}$ and $\ddot{\Psi}$ are the first and second differential of yaw angle, Ψ. Likewise, $\dot{\phi}$ and $\ddot{\phi}$ are the first and second differential of roll angle, ϕ, respectively. The other parameter values can be seen in Table 2, Table 6 [16], and FIGURE 4.

In addition, the change rate of Euler angle and rotational angular velocity of the UAV with the small interference can be seen as the same, so we can obtain the following result:

$$\begin{aligned} Y_{\dot{\phi}} &= Y_P; \quad Y_{\dot{\psi}} = Y_r; \quad L_{\dot{\phi}} = L_p; \\ L_{\dot{\psi}} &= L_r; \quad N_{\dot{\phi}} = N_p; \quad N_{\dot{\psi}} = N_r \end{aligned}$$

Then, using the Laplace transformation to Eq. (10) and assuming the initial conditions are zero; also the initial flying state of the system is stable; therefore, we can also get the following result:

$$\begin{aligned} &\mathcal{L}(\delta_A) = \delta_A(s); \quad \mathcal{L}(\delta_R) = \delta_R(s) \\ &\mathcal{L}(\beta) = \beta(s); \quad \mathcal{L}(\dot{\beta}) = s\beta(s) \\ &\mathcal{L}(\phi) = \phi(s); \quad \mathcal{L}(\dot{\phi}) = \mathcal{L}(p) = s\phi(s); \\ &\mathcal{L}(\ddot{\phi}) = \mathcal{L}(\dot{p}) = s^2\phi(s) \\ &\mathcal{L}(\psi) = \psi(s); \quad \mathcal{L}(\dot{\psi}) = \mathcal{L}(r) = s\psi(s); \\ &\mathcal{L}(\ddot{\psi}) = \mathcal{L}(\dot{r}) = s^2\psi(s) \end{aligned}$$

TABLE 5. Partial derivatives of longitudinal aerodynamics for Scale Cessna 182 [16].

Parameter	Value
X_{u_S}	-0.07839
X_{w_S}	0.228
M_{q_S}	-11.1841
Z_{u_S}	-0.75274
Z_{w_S}	-5.4448
Z_{q_S}	-1.7613
M_{u_S}	0
M_{w_S}	-1.5005
$M_{\dot{w}_S}$	-0.0771
X_{α_S}	19.459
X_{δ_S}	0
$Z_{\dot{\alpha}_S}$	-0.7678
Z_{α_S}	-464.71
Z_{δ_S}	-44.985
$M_{\dot{\alpha}_S}$	-6.584
M_{α_S}	-128.079
M_{δ_S}	-234.419
$X_{T_{u_S}}$	-0.0392
$M_{T_{u_S}}$	*0*
$M_{T_{\alpha_S}}$	*0*

TABLE 6. Relationships for partial derivatives of lateral aerodynamics [16].

	Side force of Y axis	Slip moment of L-X axis	Yaw moment of N-Z axis
Sideslip angle (β)	Y_β	L_β	N_β
Speed of roll angle (p)	Y_p	L_p	N_p
Speed of yaw angle (r)	Y_r	L_r	N_r
Aileron angle (δ_A)	Y_{δ_A}	L_{δ_A}	N_{δ_A}
Rudder angle (δ_R)	Y_{δ_R}	L_{δ_R}	N_{δ_R}

Set $I_1 = \frac{I_{XZ}}{I_{XX}}$, $I_2 = \frac{I_{XZ}}{I_{ZZ}}$, and substitute I_1 and I_2 to the Eq. (10), we can get Eq. (11) as follows:

$$\begin{aligned}&(s\boldsymbol{V_{P1}}-\boldsymbol{Y_\beta})\boldsymbol{\beta}(s)-(s\boldsymbol{Y_p}+\boldsymbol{gcos\Theta_1})\boldsymbol{\phi}(s)+s(\boldsymbol{V_{P1}}-\boldsymbol{Y_r})\boldsymbol{\psi}(s)\\&=\boldsymbol{Y_\delta}\boldsymbol{\delta}(s)-\boldsymbol{L_\beta}\boldsymbol{\beta}(s)+s(s-\boldsymbol{L_P})\boldsymbol{\phi}(s)-s(s\boldsymbol{I_1}+\boldsymbol{L_r})\boldsymbol{\psi}(s)\\&=\boldsymbol{L_\delta}\boldsymbol{\delta}(s)-\boldsymbol{N_\beta}\boldsymbol{\beta}(s)-s(s\boldsymbol{I_2}+\boldsymbol{N_p})\boldsymbol{\phi}(s)+s(s-\boldsymbol{N_r})\boldsymbol{\psi}(s)\\&=\boldsymbol{N_\delta}\boldsymbol{\delta}(s)\end{aligned} \tag{11}$$

In the aircraft motion, let the aileron angle $\delta_A(t)$ and rudder angle $\delta_R(t)$ be the inputs of the lateral motion. Therefore, the transfer functions of the lateral motion are $\left\{\frac{\beta(s)}{\delta_R(s)}, \frac{\phi(s)}{\delta_A(s)}, \frac{\psi(s)}{\delta_R(s)}\right\}$. After reintegrating Eq. (11), we can get a result as Eq. (12) [12]:

$$\begin{bmatrix}\left(s\boldsymbol{V_{P_1}}-\boldsymbol{Y_\beta}\right) & -\left(s\boldsymbol{Y_p}+\boldsymbol{gcos\Theta_1}\right) & s\left(\boldsymbol{V_{P_1}}-\boldsymbol{Y_r}\right)\\ -\boldsymbol{L_\beta} & s\left(s-\boldsymbol{L_p}\right) & -s\left(s\boldsymbol{I_1}+\boldsymbol{L_r}\right)\\ -\boldsymbol{N_\beta} & -s\left(s\boldsymbol{I_2}+\boldsymbol{N_p}\right) & s\left(s-\boldsymbol{N_r}\right)\end{bmatrix}$$

$$\begin{Bmatrix}\frac{\boldsymbol{\beta}(s)}{\boldsymbol{\delta_R}(s)}\\ \frac{\boldsymbol{\phi}(s)}{\boldsymbol{\delta}_{\mathrm{A}}(s)}\\ \frac{\boldsymbol{\psi}(s)}{\boldsymbol{\delta_R}(s)}\end{Bmatrix} = \begin{Bmatrix}\boldsymbol{Y_{\delta_R}}\\ \boldsymbol{L_{\delta_A}}\\ \boldsymbol{N_{\delta_R}}\end{Bmatrix} \tag{12}$$

Applying Cramer theory with Eq. (12) again, we can rearrange the transfer function as Eq. (13)-Eq. (15):

$$\frac{\boldsymbol{\beta}(s)}{\boldsymbol{\delta_R}(s)} = \frac{\begin{vmatrix}\boldsymbol{Y_{\delta_R}} & -(s\boldsymbol{Y_p}+\boldsymbol{gcos\Theta_1}) & s(\boldsymbol{V_{P_1}}-\boldsymbol{Y_r})\\ \boldsymbol{L_{\delta_A}} & s(s-\boldsymbol{L_p}) & -s(s\boldsymbol{I_1}+\boldsymbol{L_r})\\ \boldsymbol{N_{\delta_R}} & -s(s\boldsymbol{I_2}+\boldsymbol{N_p}) & s(s-\boldsymbol{N_r})\end{vmatrix}}{\begin{vmatrix}(s\boldsymbol{V_{P_1}}-\boldsymbol{Y_\beta}) & -(s\boldsymbol{Y_p}+\boldsymbol{gcos\Theta_1}) & s(\boldsymbol{V_{P_1}}-\boldsymbol{Y_r})\\ -\boldsymbol{L_\beta} & s(s-\boldsymbol{L_p}) & -s(s\boldsymbol{I_1}+\boldsymbol{L_r})\\ -\boldsymbol{N_\beta} & -s(s\boldsymbol{I_2}+\boldsymbol{N_p}) & s(s-\boldsymbol{N_r})\end{vmatrix}} \tag{13}$$

$$\frac{\boldsymbol{\phi}(s)}{\boldsymbol{\delta_A}(s)} = \frac{\begin{vmatrix}(s\boldsymbol{V_{P_1}}-\boldsymbol{Y_\beta}) & \boldsymbol{Y_{\delta_R}} & s(\boldsymbol{V_{P_1}}-\boldsymbol{Y_r})\\ -\boldsymbol{L_\beta} & \boldsymbol{L_{\delta_A}} & -s(s\boldsymbol{I_1}+\boldsymbol{L_r})\\ -\boldsymbol{N_\beta} & \boldsymbol{N_{\delta_R}} & s(s-\boldsymbol{N_r})\end{vmatrix}}{\begin{vmatrix}(s\boldsymbol{V_{P_1}}-\boldsymbol{Y_\beta}) & -(s\boldsymbol{Y_p}+\boldsymbol{gcos\Theta_1}) & s(\boldsymbol{V_{P_1}}-\boldsymbol{Y_r})\\ -\boldsymbol{L_\beta} & s(s-\boldsymbol{L_p}) & -s(s\boldsymbol{I_1}+\boldsymbol{L_r})\\ -\boldsymbol{N_\beta} & -s(s\boldsymbol{I_2}+\boldsymbol{N_p}) & s(s-\boldsymbol{N_r})\end{vmatrix}} \tag{14}$$

$$\frac{\boldsymbol{\psi}(s)}{\boldsymbol{\delta_R}(s)} = \frac{\begin{vmatrix}(s\boldsymbol{V_{P_1}}-\boldsymbol{Y_\beta}) & -(s\boldsymbol{Y_p}+\boldsymbol{gcos\Theta_1}) & \boldsymbol{Y_{\delta_R}}\\ -\boldsymbol{L_\beta} & s(s-\boldsymbol{L_p}) & \boldsymbol{L_{\delta_A}}\\ -\boldsymbol{N_\beta} & -s(s\boldsymbol{I_2}+\boldsymbol{N_p}) & \boldsymbol{N_{\delta_R}}\end{vmatrix}}{\begin{vmatrix}(s\boldsymbol{V_{P_1}}-\boldsymbol{Y_\beta}) & -(s\boldsymbol{Y_p}+\boldsymbol{gcos\Theta_1}) & s(\boldsymbol{V_{P_1}}-\boldsymbol{Y_r})\\ -\boldsymbol{L_\beta} & s(s-\boldsymbol{L_p}) & -s(s\boldsymbol{I_1}+\boldsymbol{L_r})\\ -\boldsymbol{N_\beta} & -s(s\boldsymbol{I_2}+\boldsymbol{N_p}) & s(s-\boldsymbol{N_r})\end{vmatrix}} \tag{15}$$

Considering the scale factor between the scale Cessna 182 and the prototype Cessna 182 [10]–[12] and the partial derivatives of lateral aerodynamics [9], [15], we can get the partial derivative value in proportion as Table 7 and Table 8 [12]. After reintegrating and deriving Eq. (11) with the parameters in Table 6-8, we can also obtain three transfer functions of the lateral motion for scale Cessna 182 (shown as Eq. (16–18) [12]):

Transfer function from the rudder angle ($\delta_{R_s}(s)$) to the sideslip angle ($\beta_s(s)$), (16), as shown at the bottom of the next page.

Transfer function from the aileron angle ($\delta_{A_s}(s)$) to the roll angle ($\phi_s(s)$), (17) as shown at the bottom of the next page.

Transfer function from the rudder angle ($\delta_{R_s}(s)$) to the yaw angle ($\psi_s(s)$), (18) as shown at the bottom of the next page.

E. TRANSFER FUNCTION OF THE ACTUATOR

Essentially, when analyzing the aircraft system, we should consider the effect of the actuator. Basically, the actuator is a first order system. Its transfer function can be represented as Eq. (19), and the parameters of the actuator are shown as Table 9.

$$\frac{\delta}{\nu} = \frac{\boldsymbol{K_a}}{\boldsymbol{\tau}s+\mathbf{1}} \tag{19}$$

TABLE 7. The ratios of longitudinal aerodynamics for Scale Cessna 182 [12].

Parameter	Scale factor SF=6.65
Y_β/Y_{β_S}	1
$L_{\delta_A}/L_{\delta_{AS}}$	SF
L_β/L_{β_S}	SF
$N_{\delta_A}/N_{\delta_{AS}}$	SF
N_β/N_{β_S}	SF
$Y_{\delta_R}/Y_{\delta_{RS}}$	1
Y_p/Y_{P_S}	$\sqrt{1/SF}$
$L_{\delta_R}/L_{\delta_{RS}}$	SF
L_p/L_{p_S}	$1/\sqrt{1/SF}$
$N_{\delta_R}/N_{\delta_{RS}}$	SF
N_p/N_{p_S}	$1/\sqrt{1/SF}$
L_r/L_{r_S}	$1/\sqrt{1/SF}$
Y_r/Y_{r_S}	$\sqrt{1/SF}$
N_r/N_{r_S}	$1/\sqrt{1/SF}$

TABLE 8. Partial derivatives of lateral motion for Scale Cessna 182 [12].

Parameter	Value
Y_{β_S}	-41.11
Y_{r_S}	0.71
$Y_{\delta_{RS}}$	19.56
L_{β_S}	-201.163
L_{r_S}	-5.5185
$L_{\delta_{RS}}$	32.053
N_{β_S}	61.6455
N_{r_S}	-3.1203
$N_{\delta_{RS}}$	-67.7635
Y_{p_S}	-0.249
$Y_{\delta_{AS}}$	0
N_{p_S}	-0.9284
L_{p_S}	-33.4465
$L_{\delta_{AS}}$	499.149
$N_{\delta_{AS}}$	-22.6765

Typically, the initial gain value of servo motor, K_a, is set as 1, and time constant of servo motor, τ, is usually between 0.05 - 0.25 second. In this paper, we have set the value of τ as 0.1 second.

TABLE 9. Parameter of actuator.

Parameter	Quantity
δ_E	Angle of elevator
v_E	Input voltage
K_a	Gain value of servo motor
τ	Time constant of servo motor

Since the definition of each system's direction is different, there is actuator's math model definition. Because of the difference in the definition of the direct is different, a negative symbol $\frac{10}{s+10}$ must be placed in front of the actuator transfer function.

In addition, the up direction with respect to the surfaces of the elevator and rudder is negative in definition. However, the up direction with respect to the aileron surface is the opposite.

Hence, the transfer functions of servo motors for elevator, rudder, and aileron can be defined as Eq. (20):

$$\begin{cases} \textbf{For Elevator}: G\dfrac{\delta_E}{v_E} = -\dfrac{10}{s+10} \\ \textbf{For Rudder}: G\dfrac{\delta_R}{v_R} = -\dfrac{10}{s+10} \\ \textbf{For Aileron}: G\dfrac{\delta_A}{v_A} = \dfrac{10}{s+10} \end{cases} \tag{20}$$

Finally, there are two reasons not mentioned regarding the actuator saturation problem:

1) This paper is a comprehensive analysis of the characteristics of different subsystems in drones, and completes the controller design of each subsystem to improve the system response. The experiment is verified by the software simulation results, but the saturation phenomenon of the actuator entity is temporarily not taken into account for the time being. In the future, when the UAV hardware integration and measurement are performed, the actuators assigned to each subsystem and their actual different saturation phenomena will be included in the design considerations of the controller, and it will even be realistically possible for the UAVs to face the interference data (such as the atmospheric model) and

$$\frac{\beta_s(s)}{\delta_{R_s}(s)} = \frac{19.56s^4 + 10483.9816s^3 + 1387923.0948s^2 - 17870.931s}{85.3511s^5 + 20795.8516s^4 + 428413.4354s^3 + 1466182.8401s^2 + 18755.221s} \tag{16}$$

$$\frac{\phi_s(s)}{\delta_{A_s}(s)} = \frac{42602.9162s^3 + 833502.2803s^2 + 2609905.1943s}{85.3511s^5 + 20795.8516s^4 + 428413.4354s^3 + 1466182.8401s^2 + 18755.221s} \tag{17}$$

$$\frac{\psi_s(s)}{\delta_{R_s}(s)} = \frac{-5783.6893s^3 - 1304871.8347s^2 - 332356.8248s - 114340}{85.3511s^5 + 20795.8516s^4 + 428413.4354s^3 + 1466182.8401s^2 + 18755.221s} \tag{18}$$

also have it incorporate into the system-wide integrated design.

2) In the study of the design of UAV motion controllers, most of the software simulations do not consider the saturation of the actuators for the time being. Only a few studies have specifically simulated the saturation phenomenon of the actuators because of special issues. However, C.-Y. Yang [12], the main object of comparison in this paper, and other literature on the design of unmanned aerial vehicle controllers, are the last to carry out experimental verification of software simulation. As far as we know, none of them are incorporating saturation of actuator hardware into software simulation design. Therefore, in order to carry out a fair controller design comparison and contrast, we decided not to consider the saturation of the actuator in the paper for the time being, so that our design can have the same system architecture and experimental scene as other comparative documents, and subsequently get the better response of system which can highlight the superiority of the controller design in this study.

III. PARAMETRIC ANALYSIS

This study is based on the RL and RC criterions, and is combined with various controller techniques to design the robust controllers. In addition, different from other references that use Ziegler–Nichols method or another trial and error method to obtain the PID parameters, in this paper, the methods of the controller designs are more flexible and adjustable when trying to achieve desired responses.

In this paper, controller design, firstly, applies the RL to find the impact of a single variable change. Secondly, it uses the RC to solve the coupling effects among the multiple controller parameters and to go further into finding the optimal parameters of the controllers. Furthermore, we propose a new design method of controller with the reverse multi-variable RC. This new method is practical and efficient when designing the controllers. It can also overcome the negative effects that result from the non-minimum phase system, of which Ziegler–Nichols method or other design methods cannot deal with. Even though there are already some methods that have been applied to handle the problems that come from the non-minimum phase system, e.g., fuzzy PID, sliding mode control, multi-model adaptive control, and so on [18]–[21], these methods are rarely used to help stabilizing the aircrafts or applied to avoid obstacles and perform some tasks. On the contrary, the new method in this paper certainly improves both the transient response and the steady-state performance. It can overcome the difficulties of the controller design that stem from the high-order aircraft systems and the non-minimum phase systems. Besides, it also helps in designing suitable controllers to meet the task requirements and extend the UAV applications. The following are the descriptions of the controller designs in this research.

TABLE 10. Ziegler–Nichols method.

Controller	K_p	K_i	K_d
P	$0.5K_u$	0	0
PI	$0.45K_u$	$0.45\,K_u/0.83T_u$	0
PID	$0.60K_u$	$0.6K_u/0.5T_u$	$0.6K_u/0.125T_u$

A. ZIEGLER-NICHOLS METHOD

The Ziegler-Nichols method is created by two engineers of Taylor Instrument. The method is used to obtain the approximate value of PID parameters. The first step of Ziegler-Nichols method is to set both the integration gain $\mathbf{K_i}$ and differential gain $\mathbf{K_d}$ as "0 ", then gradually increase the value of proportional gain $\mathbf{K_p}$ from zero to its maximum value $\mathbf{K_u}$. At this time, the output of the controller will oscillate by a constant value, and its oscillation period is $\mathbf{T_u}$. Then the maximum value $\mathbf{K_u}$ and the oscillation period $\mathbf{T_u}$ are used to obtain the PID controller parameter according to the types of controllers (shown in Table 10). Indeed, the controller parameters will not be accurate; hence the users have to implement the trial and error method to revise the response. However, many PID designers use Ziegler-Nichols method to replace the orthodox PID method whose design process has to be combined with RL or RC. Although Ziegler-Nichols method is too easy, it is too irregular and inaccurate compared to the expected value. When facing unexpected situations, it lacks the flexibility to immediately adjust one specific or all of the controller parameters to handle the situation.

This is the most significant disadvantage of the Ziegler-Nichols method. Besides, the Ziegler-Nichols method can't be used with non-minimum phase or unstable systems. Nevertheless, there are many coupling effects among the forces and moments of the aircrafts. A non-minimum phase system always exists. It makes the whole system diverge and become unstable. In this case, Ziegler-Nichols method can't solve the problem, so that is the main reason why we created a new design method based on RC to overcome the non-minimum phase problem as mentioned in this paper.

B. PID CONTROLLER

The advantages of the orthodox PID controller include: (1) PID is theoretical; (2) it is easy to achieve; (3) it has high control accuracy. However, the controller designers must deeply understand the system characteristics and the operating environments. Moreover, these PID controllers must be designed via RL and RC criterions, and then operators can design the suitable PID controllers. However, now there are many operators' designs that apply the Ziegler–Nichols method to design the PID controllers. Therefore, these PID controllers lack the advantages of the orthodox PID discussed above. The greatest strength of these PID based on Ziegler–Nichols method is that it is easier to obtain the PID parameters. Even though these parameters are not very appropriate,

TABLE 11. Parameter of PID controller.

Parameter	Quantity
K_p	Proportional gain
K_i	Integral gain
K_d	Derivative gain
e	Error
T	Time
τ	Variable of integration

these parameters have helped to make some slight improvements towards better system performance; also, the operators do not have to learn the additional design techniques of the orthodox PID controller, e.g., RL, RC, and so on. However, the Ziegler–Nichols method really lacks flexibility and accuracy. It is not easy to adjust some specific parameters to meet some special demands or achieve some special accuracy in real time. It's just a kind of trial and error method where one has to try many times to slightly improve the performance. This is also the main reason why we didn't apply the easier Ziegler–Nichols method to design PID or other controllers in this paper.

The general form of PID transfer function is shown as Eq. (21), where the related parameters can be seen in Table 10.

$$u_{PID}(t) = K_p e(t) + K_i \int_0^t e(\tau)\, dt + K_d \frac{de(t)}{dt} \quad (21)$$

The ideal PID controller can be seen as the aggregation of two zeros and one pole which is located at the origin of s-plane. It belongs to an active circuit, which can be used to improve the system transient response and steady-state error at the same time.

Because the RL can just select one controller parameter at a time when designing PID controller, it's usually divided into two steps: (1) PD controller improves the system transient response; and (2) PI controller improves the steady state error of the system. These two steps are not prioritized. In addition, using RL does help to find the optimal poles and zeros of the closed-loop system. The rule is that the total angel summation of poles and zeros located at the root locus has to be $\mathbf{180^\circ}$ (shown in FIGURE 5). Besides, according to our past experiences, after finding one parameter, we suggest that designers should simulate before searching for the next parameter. Also, after obtaining the whole controller parameters, designers still need to pay attention to the root sensitiveness and the coupling effects among the parameters.

In addition, if we have to adjust the controller parameters to suddenly meet the new requirement of the tasks, in accordance with our past working experience, the parameters' adjustment of the PID controller can approximately comply with the Table 12. Designing controllers needs to consider a number of factors that may affect the system performances, not just obtain the controller parameters based on the Ziegler-Nichols method. This is also why our controller designs are more flexible than Ziegler-Nichols method or other designs.

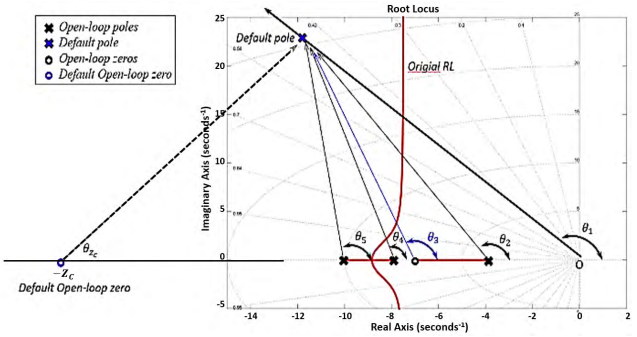

FIGURE 5. The total angel summation of poles and zeros located at the root locus must equal an odd multiple of 180°.

TABLE 12. Principles of PID controller design.

Characteristic	$\uparrow K_p$	$\uparrow K_i$	$\uparrow K_d$
Rise time	Decline	Slightly Decline	Slightly Decline
Setting time	Slightly Increase	Increase	Decline
Overshoot	Increase	Increase	Decline
$\mathbf{e}(\infty)$	Decline	Suddenly Decline	The Same
Stability	Decline	Decline	Increase

C. ROOT CONTOURS METHOD

The best assistant tool of PID controller is the root locus method (RL). It can help designers to obtain the desired characteristic roots or estimate the trend of the future system responses by the change of a single variable (e.g., gain or other variables).

However, while the system has no only one variable, we need another method to use in response to multiple variables. This design method is called as "root contour" (RC). It can deal with the design problems of the multiple variables. The following is the brief description of the RL and RC:

1) RL: if the open-loop transfer function of the system is shown as Eq. (22):

$$G(s)H(s) = KG_1(s)H_1(s) = \frac{KR_1(s)}{Q_1(s)}$$
$$\begin{cases} Q_1(s) = s^n + a_{n-1}s^{n-1} + \ldots + a_1 s + a_0 \\ R_1(s) = s^m + b_{m-1}s^{m-1} + \ldots + b_1 s + b_0 \\ a_1, Aa_2, A\ldots, Aa_n, Ab_1, Ab_2, A\ldots, Ab_n \\ \quad \textbf{is fixed real number} \\ K = \textbf{is constant}, -\infty < K < \infty \end{cases} \quad (22)$$

Eq. (22) is also the general form of RL. At the same time, the closed-loop transferring function of the system is shown as Eq. (23): is also the general form of RL. At the same time, the closed-loop transferring function of the system is shown

as Eq. (23):

$$\frac{\boldsymbol{Y}(\boldsymbol{s})}{\boldsymbol{R}(\boldsymbol{s})} = \frac{\boldsymbol{KG}(\boldsymbol{s})}{1 + \boldsymbol{G}(\boldsymbol{s})\boldsymbol{H}(\boldsymbol{s})} \tag{23}$$

Where $\boldsymbol{Y}(\boldsymbol{s})$ is the system output, $\boldsymbol{R}(\boldsymbol{s})$ is the reference input. From Eq. (23), we can find that the system characteristic equation is shown in Eq. (24):

$$1 + \boldsymbol{G}(\boldsymbol{s})\boldsymbol{H}(\boldsymbol{s}) = 0 \tag{24}$$

By integrating Eq. (22) and (24), we can get Eq. (25):

$$\boldsymbol{Q_1}(\boldsymbol{s}) + \boldsymbol{KR_1}(\boldsymbol{s}) = 0 \tag{25}$$

By dividing both sides by the term which doesn't include the variable $\boldsymbol{K}$, we can get Eq. (26):

$$1 + \frac{\boldsymbol{KR_1}(\boldsymbol{s})}{\boldsymbol{Q_1}(\boldsymbol{s})} = 0 \tag{26}$$

After obtaining $\boldsymbol{Q_1}(\boldsymbol{s})$ and $\boldsymbol{R_1}(\boldsymbol{s})$, we can use RL to obtain the controller parameters.

For example, if a characteristic equation of system is shown in Eq. (27), we can get:

$$\boldsymbol{s}(\boldsymbol{s}+1)(\boldsymbol{s}+2) + \boldsymbol{K}(\boldsymbol{s}+1)\boldsymbol{s} + (\boldsymbol{s}+2) = 0 \tag{27}$$

By dividing both sides with the term: $[\boldsymbol{s}(\boldsymbol{s}+1)(\boldsymbol{s}+2) + (\boldsymbol{s}+2)]$ in Eq. (27), we can get Eq. (28):

$$1 + \frac{\boldsymbol{K}(\boldsymbol{s}+1)\boldsymbol{s}}{\boldsymbol{s}(\boldsymbol{s}+1)(\boldsymbol{s}+2) + (\boldsymbol{s}+2)} = 0 \tag{28}$$

By comparing Eq. (28) with Eq. (26), we can easily get the result as shown in Eq. (29).

$$\frac{\boldsymbol{R_1}(\boldsymbol{s})}{\boldsymbol{Q_1}(\boldsymbol{s})} = \frac{(\boldsymbol{s}+1)\boldsymbol{s}}{\boldsymbol{s}(\boldsymbol{s}+1)(\boldsymbol{s}+2) + (\boldsymbol{s}+2)} \tag{29}$$

Therefore, according to Eq. (22) and (29), we can get Eq. (30):

$$\boldsymbol{G}(\boldsymbol{s})\boldsymbol{H}(\boldsymbol{s}) = \frac{\boldsymbol{KR_1}(\boldsymbol{s})}{\boldsymbol{Q_1}(\boldsymbol{s})} \tag{30}$$

So we can use the root locus method to design the controller, too.

2) RC is the extended criterion from RL that is used to deal with the multiple-variables problem. RC criterion can be summarized as following:

Since the characteristic polynomial is 0, we can assume that a closed-loop system has two variables in the characteristic polynomial. RC general form is shown as Eq. (31). This form is similar to Eq. (25).

$$\boldsymbol{Q}(\boldsymbol{s}) + \boldsymbol{K_1R_1}(\boldsymbol{s}) + \boldsymbol{K_2R_2}(\boldsymbol{s}) = 0 \tag{31}$$

The First step of RC is to set any one of the variables to zero. In this description, we set variable $\boldsymbol{K_2}$ to 0, then Eq. (31) can be rewritten as Eq. (32):

$$\boldsymbol{Q}(\boldsymbol{s}) + \boldsymbol{K_1R_1}(\boldsymbol{s}) = 0 \tag{32}$$

We divide both sides of Eq. (32) by the term that does not contain the variable $\boldsymbol{K_1}$, then we can get Eq. (33):

$$1 + \frac{\boldsymbol{K_1R_1}(\boldsymbol{s})}{\boldsymbol{Q}(\boldsymbol{s})} = \frac{\boldsymbol{Q}(\boldsymbol{s}) + \boldsymbol{K_1R_1}(\boldsymbol{s})}{\boldsymbol{Q}(\boldsymbol{s})} = 0 \tag{33}$$

Form Eq. (33), we can find the general form of RL as the term: $\frac{\boldsymbol{K_1R_1}(\boldsymbol{s})}{\boldsymbol{Q}(\boldsymbol{s})}$, then we draw the RL based on the variable $\boldsymbol{K_1}$ according to Eq. (33). This is the first RL in this multiple-variables system.

Secondly, in Eq. (31), we set $\boldsymbol{K_1}$ as a random constant, and $\boldsymbol{K_2}$ becomes the new system variable now. We divide both sides in Eq. (31) by the term that does not contain the variable $\boldsymbol{K_2}$, then we can get Eq. (34):

$$1 + \frac{\boldsymbol{K_2R_2}(\boldsymbol{s})}{\boldsymbol{Q}(\boldsymbol{s}) + \boldsymbol{K_1R_1}(\boldsymbol{s})} = \frac{\boldsymbol{Q}(\boldsymbol{s}) + \boldsymbol{K_1R_1}(\boldsymbol{s}) + \boldsymbol{K_2R_2}(\boldsymbol{s})}{\boldsymbol{Q}(\boldsymbol{s}) + \boldsymbol{K_1R_1}(\boldsymbol{s})} = 0 \tag{34}$$

At this time, the variable of the system is $\boldsymbol{K_2}$ and $\boldsymbol{K_1}$ is a constant. In Eq. (34), we can also find the other general form of RL as Eq. (35):

$$\boldsymbol{G_2}(\boldsymbol{s})\boldsymbol{H_2}(\boldsymbol{s}) = \frac{\boldsymbol{K_2R_2}(\boldsymbol{s})}{\boldsymbol{Q}(\boldsymbol{s}) + \boldsymbol{K_1R_1}(\boldsymbol{s})} \tag{35}$$

According to Eq. (35), we draw the RL with the variable $\boldsymbol{K_2}$. After finishing the first RL of the variable $\boldsymbol{K_2}$, we repeat the second step several times. We continue to set $\boldsymbol{K_1}$ as different constant values, and $\boldsymbol{K_2}$ is still the variable to draw the RL. After drawing the several RLs based on the variable $\boldsymbol{K_2}$, we can find that these RLs have the same convergence trends. Finally, we combine the total RLs including the first RL in the first step to form the root contour (RC).

By applying the RC criterion with the pole-zero properties, we can easily find the optimal parameters of the controllers. This method can be applied to a variety of controllers because the purpose of the controller is to adjust the original poles and zeros to suitable locations and to obtain the desired responses. Each controller can be disassembled into a number of pole-zero combinations. For instance, the PI controller can be taken apart into a zero and a pole located at the origin of the s-plane. Further, the PID controller can be split into a pole and the two zeros and a pole located at the origin. RC is the criterion that helps select the optimal variable value according to the desired response. The controller parameters based on RC are always much more accurate than the ones obtained by the Ziegler-Nichols method. Also, RC is more efficient than Ziegler-Nichols method and it can also be applied to the non-minimum phase systems. Therefore, RC criterion is a practical technique for controller design and it is suitable for many kinds of the controllers. In this research, we also applied RC to help design various controllers.

Finally, with regard to RL and RC, some people may raise concerns that RL and RC are not the latest theories to help non-minimum phase effectiveness. We would like to add that: although RL and RC are, at first glance, an older control theory, they are one of the few control application theories that can clearly explain the relationship

between ''gain or variable adjustment'' and ''characteristic root change''. Nevertheless, due to the rise of the Ziegler–Nichols method, current controller designers mostly use simple Ziegler–Nichols methods to obtain controller parameters when performing PID design. However, the controller parameters used to control by this method are extremely limited, inaccurate and show a lack of application flexibility; therefore, in order to do a precise controller design, we only use RL and RC to assist controller design in this paper. In addition, in light of the fact that the Root Locus theory is mostly applied to explain the relationship between adjusting the system gain and the characteristic root changes, there is little literature explaining that when multiple parameters in the controller are all adjusted, in regards to the mutual interference generated, what is the impact of system response and stability when the parameters thereof are changed respectively.

It is important to know that when selecting the parameters of controller multivariable, each control parameter will actually influence each other. Take PID controller as an example, the increase or decrease of any constants of proportional constant, integral constant or differential constant will inevitably affect the other two working effects of the parameters, which then affect the overall output response or stability of the system. This fact should be taken into account. In particular, UAV requires a highly stable system.

RC can clearly describe the interrelationship in multiple variables, so we only use RC to assist in the design of multi-parameter controllers. Therefore, RL and RC are not the latest theories, but for the design of multiple controller parameters, in particular, the system of UAVs in this study is considered to be an excellent choice which is by no means out-of-date.

D. PHASE LEAD-LAG COMPENSATOR

The aforementioned PID controller consists of two active components of integral and differential units. However, it can achieve similar responses with the passive components. That is, the ''phase lead-lag compensator''.

''Phase lead-lag compensator'' is also called ''phase lag-lead compensator''. It consists of two passive electrical networks including the phase lead compensator and the phase lag compensator. In addition, phase lead has similar effects as the PD controller, and the function of the phase lag resembles that of PI controller. Therefore, phase lead-lag can be applied to improve the transient response and the steady-state error simultaneously. The transfer function of the phase lead-lag can be written as Eq. (36), where K is the system gain, $|z_{lead}|$ and $|p_{lead}|$ are the absolute values of the zeros and the poles of the phase lead compensator. With the same expression, the $|z_{lag}|$ and $|p_{lag}|$ are the absolute values of the zeros and the poles of the phase lag compensator. Furthermore, in the phase lead compensator, the zero location is closer to the origin than the pole. Therefore,$|z_{lead}| < |p_{lead}|$. Similarly, in the phase lag compensator, the pole location is closer to the origin than the zero. Thence, $|z_{lag}| > |p_{lag}|$.

$$C_{lead-lag}(s) = \frac{\mathrm{K} * (s + z_{lead})(s + z_{lag})}{(s + p_{lead})(s + p_{lag})} \tag{36}$$

In addition, since the phase lead-lag compensator is the passive circuit, it can be used for the systems which are system type 1. Moreover, the zeros and poles of the phase lead-lag compensator can also be applied to cancel the unnecessary or disadvantageous poles and zeros of the original system.

E. NOTCH-FILTER

When establishing the mathematic model of the system, the designers always assume that initially the system was rigid. That is, they ignore the vibration due to the complexities of the elastic component in the system. However, most of the interference of the system when operating is the vibration of the system itself, such as mechanical systems, aircraft, and so on. These vibrations mostly belong to the high frequency interferences, and and are close to the imaginary axis of the s-plane. Sometimes, they will cause the closed-loop system to be unstable. At this time, Notch filter would be a good choice to deal with this problem. According to the criterion of the pole-zero cancellation, we can design the Notch filter to delete the high-frequency complex-conjugate poles near the imaginary axis to reduce the system vibration. The transfer function of the Notch filter can be seen in Eq. (37):

$$\frac{(s + a)(s + \bar{a})}{(s + b)(s + c)}$$
$$\begin{cases} a, \bar{a}: & \textit{Conjugate zero} \\ b, c: & \textit{negative real poles or conjugate poles} \end{cases} \tag{37}$$

Where a and $\bar{a}$ are used to delete the high-frequency conjugate poles, and b, c can be designed to cancel the unnecessary zeros of the original system. If the system has no wrong zeros, b, c can be set at the positions where real parts of the poles are more than five times to the dominant poles to avoid causing the negative effects. In particular, the conjugate zeros of the Notch filter cannot be used to cancel the original poles located at right-hand side (RHS) of the s-plane. Because the relative stability of the system with RHS poles is poor, when encountering the externally environmental interferences, the system will easily become unstable, and the Notch filter will not delete the RHS poles smoothly at that time.

F. RELATIVE STABILITY STANDARD

Absolute stability means that no matter the system is stable or not, relative stability is used to give the degree of the stability or determine how close the system is to the instability region. Besides, if a system has a higher relative stability than other systems, it will have a higher probability of survival. Generally, UAV is less robust since its high system order and uncertainty of operating environment. According to the US military standard (MIL-F-9490D) [16], the design standard for the relative stability of the flight carrier has to be more

than 6dB on gain margin (G.M). In addition, after the loss verification of the system, the relative stability of the whole carrier system must be above 4.5dB.

The discrimination and calculation for relative stability can be obtained by several graphical tools in the frequency domain, such as Nyquist criterion, Bode plot, Nichols plot [22], and so on. In this research, we apply the Nichols plot by Matlab to help get the relative stability of the UAV, and in section IVB, we will also give its clear introduction.

IV. RESEARCH RESULTS

A. TRANSFER FUNCTIONS OF THE ORIGINAL SYSTEM IN [12]

1) "Elevator angle to angle of attack (AOA)" system

The transfer function from the elevator angle to AOA as Eq. (7) is shown above, and the block diagram is shown in FIGURE 6. As mentioned above, most of the users apply the Ziegler-Nichols method to design PID controller. Reference [12] is an example, too. In order to verify the effect of the controller, at first, we repeated the method of [12] to apply Ziegler-Nichols method and Table 12 to design the PID controller. Therefore, we can get the three parameters ($\boldsymbol{K_p = 2, K_i = 15}$, and $\boldsymbol{K_d = 0.29}$) of Eq. (21) to be the same as [12]. This controller equation can also represent the form such as Eq. (38):

$$\boldsymbol{C_1(s) = \frac{0.29 * (s^2 + 6.9s + 51.7)}{s}} \tag{38}$$

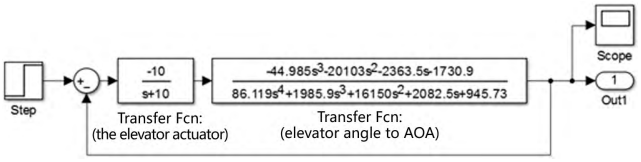

FIGURE 6. Block diagram of "elevator angle to AOA" system.

Different from other controller designs based on the Ziegler-Nichols method, we applied the RC mentioned above to design the controller so as to highlight the superiority of the designed controller in this study. We assumed that the form of PID controller is shown as Eq. (39). Especially, we set the system gain 0.29 in Eq. (39) to be the same as Eq. (38) based on the Ziegler-Nichols method. That will be a clear comparison between [12] and this study. That is also a good contrast between the Ziegler-Nichols method and our design based on RC combining with the orthodox PID criterion. Afterwards, the next procedure is to find the other parameters (K_1 and $\boldsymbol{K_2}$) of the Eq. (39):

$$\boldsymbol{C_2(s) = \frac{0.29 * (s^2 + K_1 s + K_2)}{s}} \tag{39}$$

As mentioned above, the first step is to set any one of the variables as zero. Therefore, we set $\boldsymbol{K_2 = 0}$ and $\boldsymbol{K_1}$ is a variable, and then we got the root locus (shown in FIGURE 7). In FIGURE 7, we zoomed in on the region near

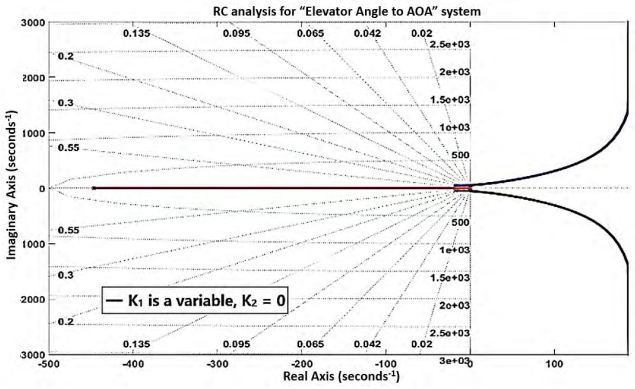

FIGURE 7. RC analysis for "elevator angle to AOA" system, $K_2 = 0$, K_1 is a variable.

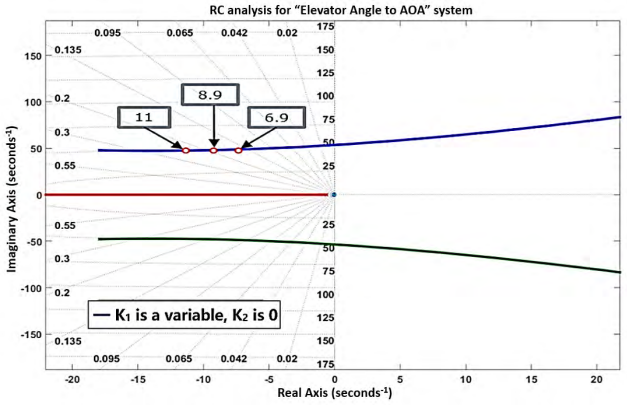

FIGURE 8. Partial enlargement around the origin point of FIGURE 7.

the origin point (shown in FIGURE 8), then we can easily figure out the root trajectory and select three parameters to be the candidates of variable $\boldsymbol{K_1}$. One of these three candidates of $\boldsymbol{K_1}$ parameter is 6.9 which is the same as [12] for comparison. However, $\boldsymbol{K_1 = 6.9}$ selected by the Ziegler-Nichols method in [12] is not perfect enough, since this point is too close to jw-axis. We randomly picked up two points, $\boldsymbol{K_1 = 8.9}$ **and** $\boldsymbol{K_1 = 11}$. According to RL criterion, all system responses of these two $\boldsymbol{K_1}$ values are much better than $\boldsymbol{K_1 = 6.9}$ taken by Ziegler-Nichols method in [12]. Besides, from the FIGURE 8, it can be seen that $\boldsymbol{K_1 = 11}$ is the leftmost half of root trajectory. Therefore, its transient response is the best compared with another two $\boldsymbol{K_1}$ values. And the transient response of $\boldsymbol{K_1 = 6.9}$ is the worst compared to another value. Table 13 also represents the three responses from the different $\boldsymbol{K_1}$.

In addition, in [12], Yang have designed the PID controller with $\boldsymbol{K_1 = 6.9}$ based on Ziegler-Nichols method. Although we can design many different values of $\boldsymbol{K_1}$ whose responses are all better than $\boldsymbol{K_1 = 6.9}$., however, the better transient response we want, the more expensive equipment we have to pay for. Hence, to avoid taking a too extreme value of $\boldsymbol{K_1}$, in this paper, we just selected the better response than $\boldsymbol{K_1 = 6.9}$, but not too extreme. Finally, we chose $\boldsymbol{K_1 = 8.9}$.

TABLE 13. Step responses from different K_1.

Characteristic	$K_1 = 6.9$	$K_1 = 8.9$	$K_1 = 11$
Peak time (sec)	11.4	8	–
Rise time (sec)	0.349	0.265	0.192
Setting time (sec)	3.61	2.63	0.6
Steady state error	0.073	0.058	0.047
Overshoot (OS%)	1.65	0.751	–

Notes: $K_2 = 0$

Of course, we can also apply our design techniques to adjust K_1 to other values according to the hardware specifications or task requirements in the future.

Continuing to the procedures of designing PID controller, the second step, K_2 is a variable, and we set $K_1 = 8.9$ as a constant value. Then we can get the root contours shown in FIGURE 9.

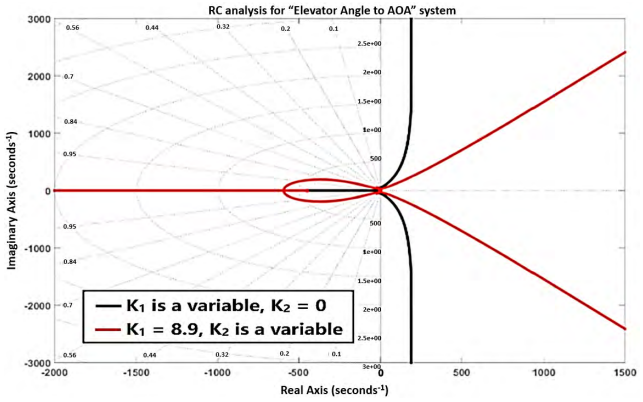

FIGURE 9. RC analysis for "elevator angle to AOA" system, where $K_1 = 8.9$, K_2 is a variable.

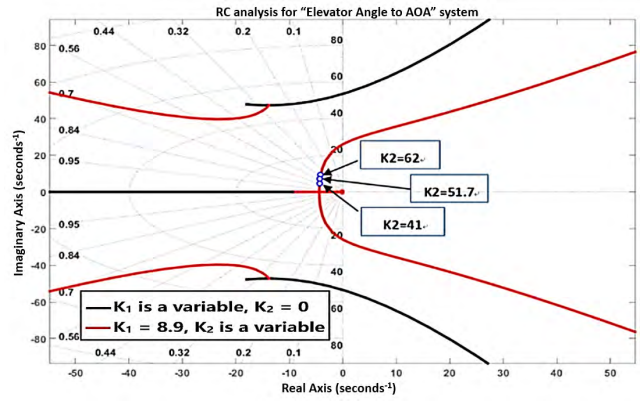

FIGURE 10. Partial enlargement around the original point from the FIGURE 9.

Again, we enlarged the region near the origin point of the FIGURE 9 to analyze the characteristic roots (shown in FIGURE 10). Since K_2 was selected as 51.7 in [12], we randomly chose another two parameters ($K_2 = 41$ and 62) around $K_2 = 51.7$ for confirmation.

In FIGURE 10, we can find that $K_2 = 41$, $K_2 = 51.7$, and $K_2 = 62$ have the similar setting time because their negative real parts are similar. However, $K_2 = 62$ has less damping ratio compared to $K_2 = 41$ and $K_2 = 51.7$. Hence, according to the property of damping ratio and RC criterion, we can predict that the system with controller parameter $K_2 = 62$ in Eq. (39) will have larger overshoots than the other two systems. Therefore, in this research, we chose a less damping ratio compared to K_2 to obtain the better transient response. The step responses of the three different K_2 can be seen in Table 14.

TABLE 14. Step responses from different K_2.

Characteristic	$K_2 = 41$	$K_2 = 51.7$	$K_2 = 62$
Peak time (sec)	0.721	4.6	0.506
Rise time (sec)	0.338	0.266	0.222
Setting time (sec)	0.977	0.868	0.775
Steady state error	0	0	0
Overshoot (OS%)	4.6	8.57	12.2

Notes: $K_1 = 8.9$

Of course, operators can always choose their optimal K_2 value according to the task requirement.

To summarize, it is possible to design a better controller for the transfer function from the elevator angle to AOA. The controller transfer function in this paper is shown as Eq. (40):

$$C_3(s) = \frac{0.29 * (s^2 + 8.9s + 41)}{s} \tag{40}$$

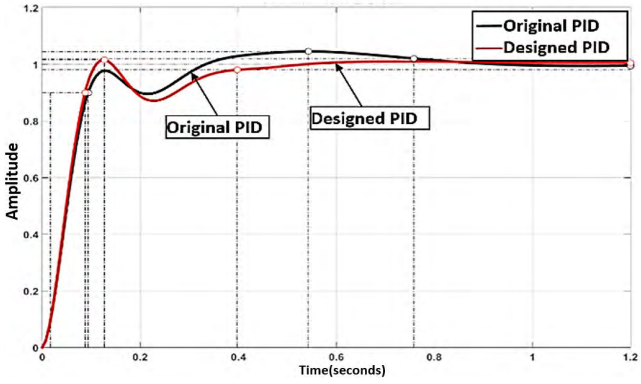

FIGURE 11. Closed-loop responses of [12] (Original PID) and our design (Designed PID).

FIGURE 11 and Table 15 are the responses of different designed PID controllers from [12] (Original PID) and our design (Designed PID). We can find that the response of the Designed PID based on RC criterion is better than the

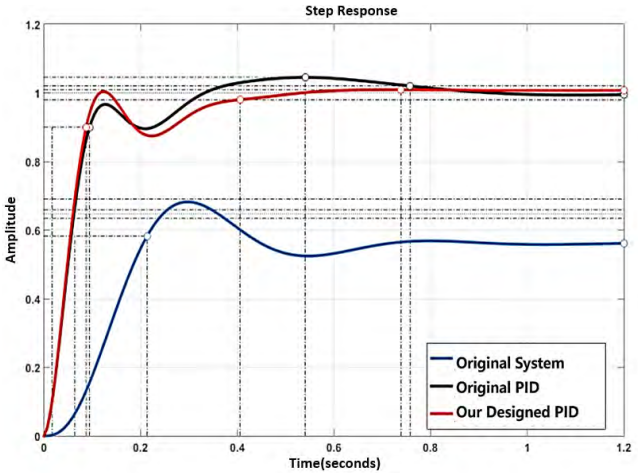

FIGURE 12. Closed-loop responses of the Original System, Original PID in [12], and Our Designed PID.

TABLE 15. The comparison of reference [12] (Original PID) and our design (Designed PID).

Characteristic	Original System	Original PID	Our Designed PID
Controller	—	$\mathbf{C_1(s)}$	$\mathbf{C_3(s)}$
Peak time (sec)	12	0.1252	0.127
Rise time (sec)	0.2	0.07	0.07
Setting time (sec)	27.5	0.7552	0.397
Steady state error	0.3533	0	0
Overshoot (OS%)	6.8045	7.2808	1.5

controller in [12] (Original PID). Besides, by comparing the controller design based on the Ziegler-Nichols method in [12], our controller design combines the orthodox PID method and RC criterion in FIGURE 11, FIGURE 12, and Table 15, not only does our design shorten the setting time of the system, but also reduce the system overshoot. It is evident that the method of controller design in this paper is effective for aircraft and UAV.

2) ''Elevator angle to speed'' system

The transfer function from the elevator angle to the speed as Eq. (8) is shown above, and the block diagram is shown in FIGURE 13. As mentioned above, most of the users apply the Ziegler–Nichols method to design PID controller. Reference [12] is an example, too. However, Yang [12] indicated that the transfer function from the elevator angle to the speed (as Eq. (7) and FIGURE 13) is unstable; the closed-loop response of Scale Cessna 182 is divergent, and the Ziegler–Nichols method could not help stabilize the system.

The pole-zero distribution of open-loop transfer function in FIGURE 13 is represented as Eq. (41):

$$\begin{cases} \boldsymbol{zero}: -\mathbf{228.84}, \mathbf{5.05} \\ \boldsymbol{pole}: -\mathbf{10}, -\mathbf{0.0618} \pm \mathbf{0.2359}\boldsymbol{i}, \\ \quad -\mathbf{11.4682} \pm \mathbf{7.2882}\boldsymbol{i} \end{cases} \tag{41}$$

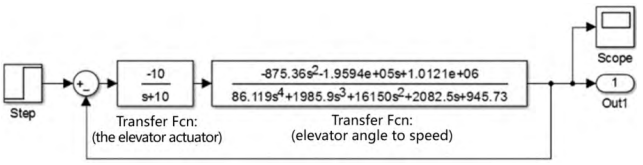

FIGURE 13. Block diagram of ''elevator angle to speed'' system.

In FIGURE 13, we tried to analyze the distribution of poles and zeros of the system. We can find that there is a zero located at RHS of the s-plane. Therefore, this is a non-minimum phase system. In addition, the step response of this closed-loop system is divergent (shown in FIGURE 14).

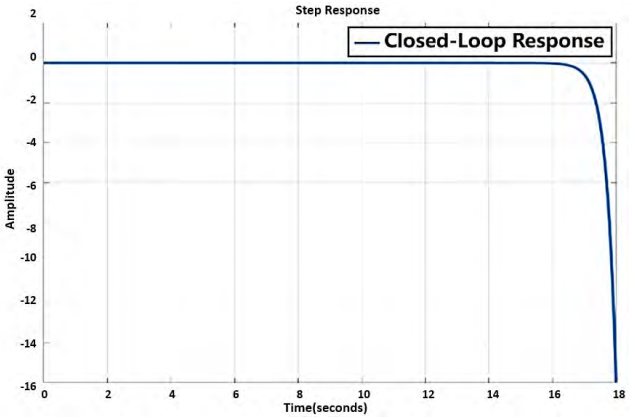

FIGURE 14. Closed-loop response of the ''elevator angle to speed'' system.

Since the system is unstable, it is impossible to find maximum gain $\boldsymbol{K_u}$ and oscillation frequency $\boldsymbol{T_u}$. Hence, the Ziegler-Nichols method is useless in helping to design the PID controller to stabilize the ''elevator angle to speed'' system. Therefore, Yang [12] also said that the unstable situation of the ''elevator angle to speed'' system cannot be handled. However, in this research, we will try to solve this problem and stabilize this system.

In the previous section (IVA1), we found that the RC can clearly illustrate the procedures of controller design and help obtain the suitable controller parameters effectively. Therefore, we applied RC to help handle the unstable system.

Again, we assumed the form of the controller as Eq. (42):

$$\boldsymbol{C_4}(s) = \frac{\boldsymbol{s^2} + \boldsymbol{K_1 s} + \boldsymbol{K_2}}{\boldsymbol{s}} \tag{42}$$

As mentioned above, the first step of design procedures in Eq. (42) is to set $\boldsymbol{K_2} = \mathbf{0}$ and $\boldsymbol{K_1}$ as a variable, then we can get the RL shown in FIGURE 15.

After zooming into the region near the origin point in FIGURE 15, it is found that there are three RLs in the RHS (FIGURE 16), so we cannot use the traditional RC to solve this problem. Since PID is the controller combined with two zeros and one pole located at the origin of the s-plane, we applied normal PID method to try to improve

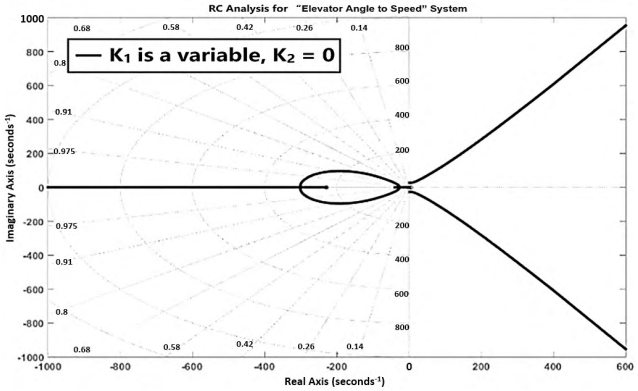

FIGURE 15. RC analysis for "elevator angle to speed" system.

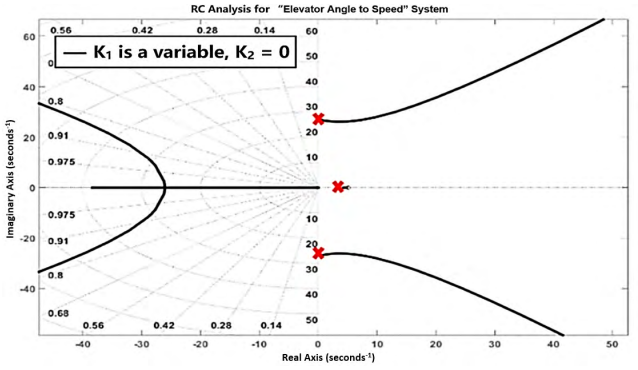

FIGURE 16. Partial enlargement around the origin point of FIGURE 15.

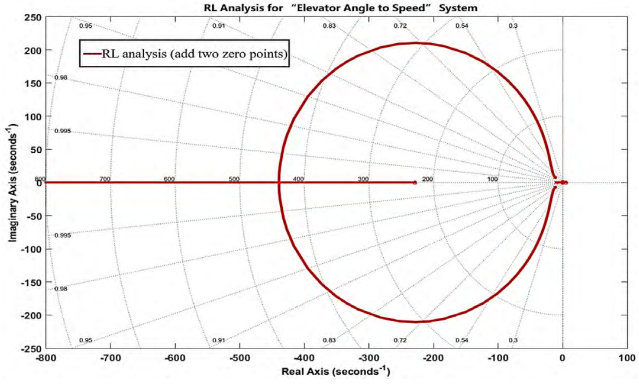

FIGURE 17. RL analysis for "elevator angle to speed" system: after adding two zeros.

this unstable system. Firstly, we added two zeros to pull the unstable trajectories back to the left-hand side (LHS) of the s-plane (shown in FIGURE 17).

Secondly, in order to reduce the steady-state error to zero, we added a pole located at the origin of the system. A system with "system type" one will have "0" steady-state error when meeting step input. However, adding a pole yields the root trajectories to the RHS of the s-plane (shown in FIGURE 18), and it worsens the transient response of the system.

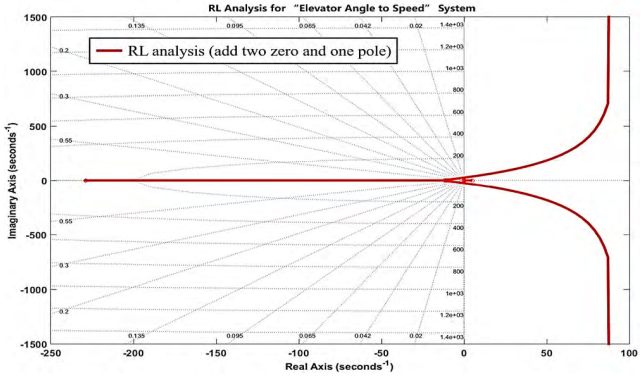

FIGURE 18. RL analysis for "elevator angle to speed" system: after adding two zeros and one pole.

According to FIGURE 14-FIGURE 18, we found that it's impossible to stabilize the "elevator angle to speed" subsystem. However, due to the analysis of the RC in FIGURE 17-FIGURE 18 we thought maybe we can add an additional compensative gain to try to stabilize the system. Therefore, we redesign the controller form from Eq. (42) to Eq. (43). Eq. (43) is the variable controller with three parameters. And the RC based on parameter $\boldsymbol{K_2}$ and $\boldsymbol{K_3}$ in Eq. (43) is the same as the RC based on $\boldsymbol{K_1}$ and $\boldsymbol{K_2}$ in Eq. (42). Besides, the additionally compensative gain $\boldsymbol{K_1}$ in Eq. (43) contributes to the effect of the parameter coupling from the $\boldsymbol{K_2}$ and $\boldsymbol{K_3}$. We chose different constant values as $\boldsymbol{K_1}$ in Eq. (43) and drew the RC based on $\boldsymbol{K_2}$ and $\boldsymbol{K_3}$ (shown in FIGURE 19-FIGURE 21). In FIGURE 19-FIGURE 21 with $\boldsymbol{K_1}$ effect, we can find that the original RC (shown in FIGURE 15) will develop along a specific trend.

$$\boldsymbol{C_5}(s) = \frac{\boldsymbol{K_1} * (s^2 + \boldsymbol{K_2}s + \boldsymbol{K_3})}{s} \tag{43}$$

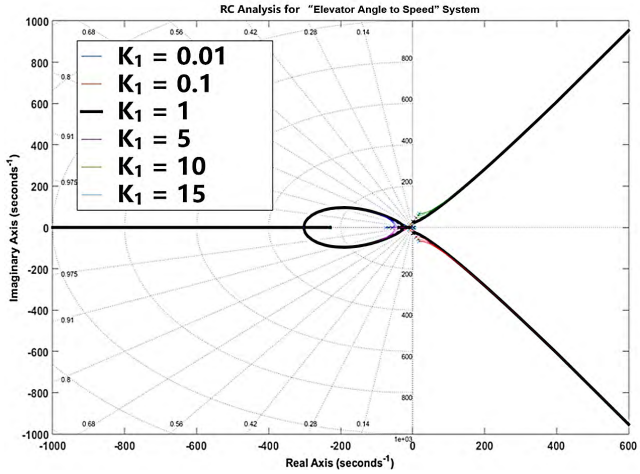

FIGURE 19. RC analysis for "elevator angle to speed" system: with additional gain K_1.

In FIGURE 19-FIGURE 21, it is obvious that there are too many characteristic roots located at RHS of s-plane.

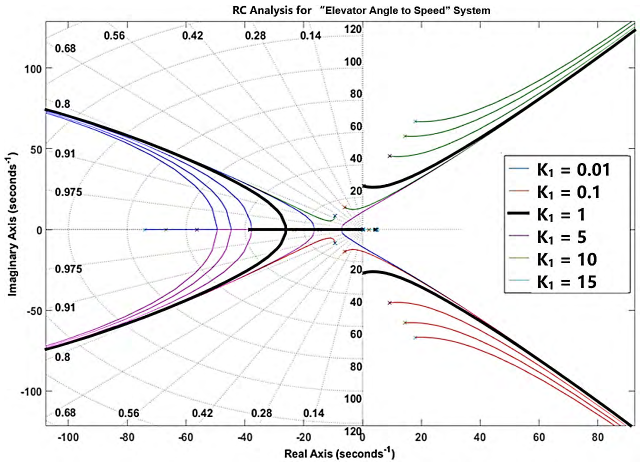

FIGURE 20. Partial enlargement around the origin point of FIGURE 19.

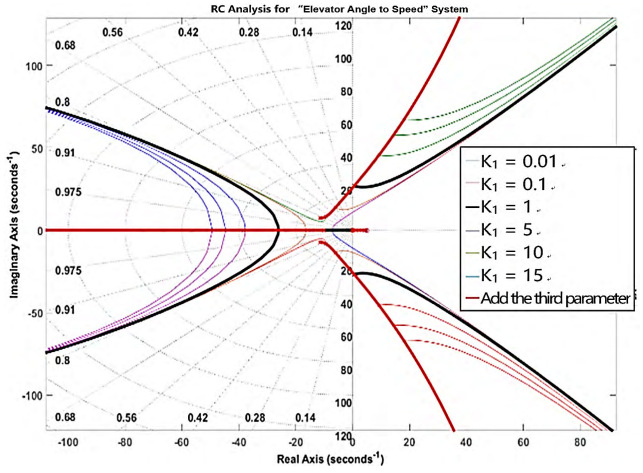

FIGURE 21. Partial enlargement and classification around the origin point of FIGURE 19.

It is impossible to improve this unstable situation by Ziegler-Nichols method. Therefore, Yang [12] has mentioned that he could not solve this problem. After analyzing this unstable system, we found that it is too complex to be handled by RC only. We can design a controller to overcome this case only via RC; however, the procedures are complicated, and sometimes, the controller parameters maybe imperfect. The first consideration in the case is how to haul the roots trajectory to the LHS of the s-plane. In view of this, we tried to create a new method to design the controller based on RC criterion. The transfer function of this new controller $\boldsymbol{C_6}(\boldsymbol{s})$ is shown as Eq. (44), and we defined this new controller as ''Reverse Gain PID Controller''. Eq. (44) has three variables too. Comparing Eq. (42) and Eq. (43), the additional gain $(-\boldsymbol{K_1})$ of Eq. (44) is designed to draw the most root trajectory in RHS of FIGURE 19 to the LHS of the s-plane.

$$\boldsymbol{C_6}(\boldsymbol{s}) = \frac{-\boldsymbol{K_1} * (\boldsymbol{s^2} + \boldsymbol{K_2 s} + \boldsymbol{K_3})}{\boldsymbol{s}} \tag{44}$$

According to Eq. (44), we started to draw the RC. Firstly, we set $\boldsymbol{K_2} = \boldsymbol{K_3} = \boldsymbol{0}$ and $\boldsymbol{K_1}$ as a variable, then we drew the RL shown in FIGURE 15. FIGURE 22 as the RL comparison of the ''elevator angle to speed'' system for different controllers with the reverse gain controller (Eq. (44)) and non-reverse gain controller (Eq. (42)). FIGURE 23 is a figure that we zoomed in on the region near the origin point in FIGURE 22. According to FIGURE 22 and FIGURE 23, it is obvious that controller with additionally reverse gain did help to yield the unstable root trajectory to the stable LHS s-plane, and improved the transient response of the system. That's why we set the controller form as Eq. (44) to deal with the ''elevator angle to speed'' system.

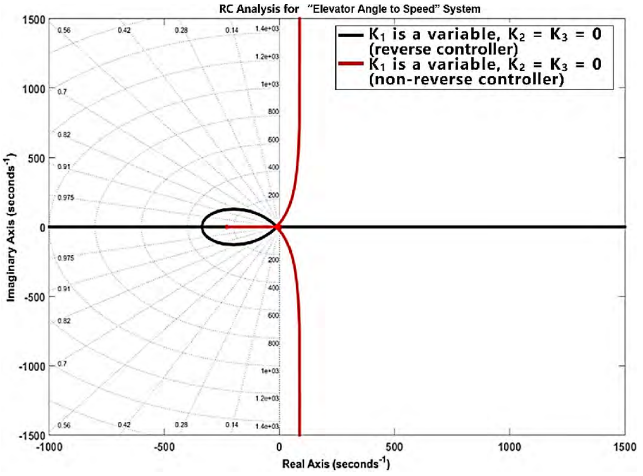

FIGURE 22. RC analysis for "elevator angle to speed" system: comparison of reverse and non - reverse controllers.

After verifying the Eq. (44) to be valid, we redesigned ''Reverse Gain PID Controller'' based on Eq. (44) for ''elevator angle to speed'' system. As mentioned above, the first step is to set all parameters as ''0'', only one parameter is the variable. Therefore, we set $\boldsymbol{K_2} = \boldsymbol{K_3} = \boldsymbol{0}$ and $\boldsymbol{K_1}$ as a variable, then we drew the root locus (shown in FIGURE 24).

In FIGURE 24, we zoomed in on the region near the origin point to easily figure out the root locus distribution (shown in FIGURE 25(a), FIGURE 25(b)). When designing $\boldsymbol{K_1}$, $\boldsymbol{K_2}$, or $\boldsymbol{K_3}$, we can always get the stable ranges and their maximum values according to the RL, RC, and Routh-Hurwitz criterions [22]. Therefore, we can find the stable range of, $\boldsymbol{K_1}$: $\boldsymbol{0 < K_1 < 0.57}$. We randomly selected three stable parameters to be candidates for variable $\boldsymbol{K_1}$, including 0.0092, 0.01805, and 0.03146. In FIGURE 25 (a), we can find that when $\boldsymbol{K_1 = 0.01805}$, the damping ratio of the system is close to 0.707, and its overshoot will be better than the one of $\boldsymbol{K_1 = 0.0092}$. In addition, even though $\boldsymbol{K_1 = 0.03146}$ seems to have less overshoot than the one of $\boldsymbol{K_1 = 0.01805}$, however, $\boldsymbol{K_1 = 0.03146}$ also leads to the system with a very small characteristic root close to the origin (shown in FIGURE 25 (b)), and this small characteristic roots will cause a large setting time. Therefore, in order to keep the fast

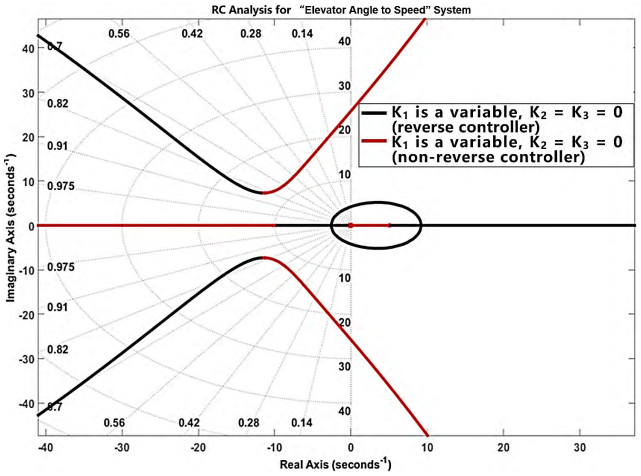

FIGURE 23. Partial enlargement around the origin point of FIGURE 22.

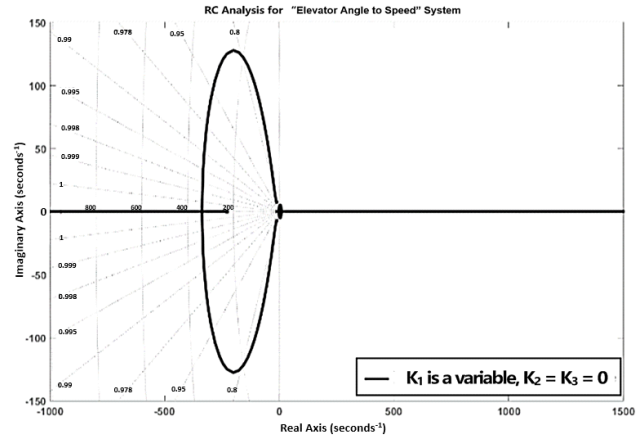

FIGURE 24. RL analysis for "elevator angle to speed" system with controller $C_6(s)$ based on variable K_1.

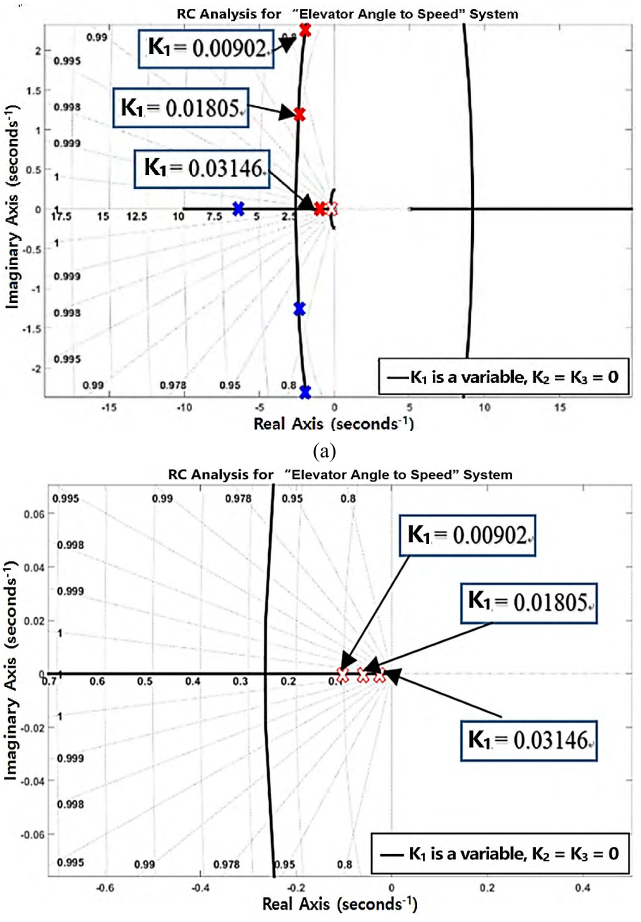

FIGURE 25. (a) Partial enlargement of FIGURE 24. (b) Partial enlargement around the origin point of FIGURE 23.

TABLE 16. $K_2 = K_3 = 0, K_1$ is a variable.

Characteristic	$K_1 = 0.00902$	$K_1 = 0.0185$	$K_1 = 0.03146$
Peak time (sec)	3.33	1.8	1.2
Rise time (sec)	0	0	0
Setting time (sec)	45.7	83..4	130
Steady state error	1	1	1

Notes: $0 < K_1 < 0.57$ for stability

response, we should choose K_1 which equals to 0.0092 or 0.01805. In this case, integrating the performance of the damping ratio and speed of the system response, we chose 0.01805 as the K_1 value in Eq. (44). And the step responses based on these three K_1 values is also shown in Table 16. Of course, the designer can also choose another different K_1 value according to the task requirements if necessary. Besides, since K_1 is the first design parameter inEq. (44), after obtaining K_1, we have to continue to design K_2 and K_3 based on K_1 value.

Therefore, the value of K_1 should be as good as possible.

The second step of the controller design for the non-minimum phase system: ''elevator angle to speed'' system is to set $K_3 = 0$, $K_1 = 0.01805$ which we selected in the first step, and K_2 is a variable. The RC with variable K_2 is shown in FIGURE 26. From RC, we can also find the stable range:$0 < K_2 < 2.2$. In FIGURE 26, we arbitrarily picked three points: 0.184, 0.495, and 0.855 as the candidates of the variable K_2. The step responses of these three acceptable K_2 values can be also seen in Table 17. By integrating the system performances of the different K_2 values, we, finally, selected $K_2 = 0.495$.

In the third step, we take K_3 as the variable. $K_2 = 0.495$ and $K_1 = 0.01805$ are the fixed constants selected in the first and second steps above. The RC based on this setting can be obtained and shown in FIGURE 27. The stable range K_3 is between 0 and 0.56. Again, we arbitrarily picked three acceptably stable parameters. These are 0.0739, 0.1255, and 0.3655, respectively. Due to the reason for the ration of the damping

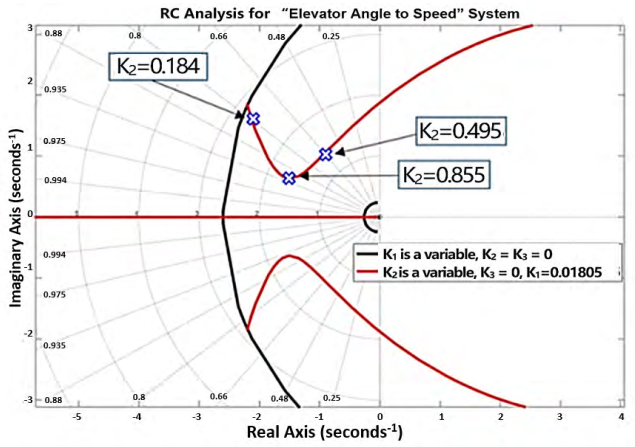

FIGURE 26. RC analysis with $K_3 = 0$, $K_1 = 0.01805$, and K_2 is a variable in Eq. (44).

TABLE 17. $K_3 = 0$, $K_1 = 0.01805$, and K_2 is a variable.

haracteristic	$K_2 = 0.184$	$K_2 = 0.495$	$K_2 = 0.855$
Peak time (sec)	—	—	3.09
Rise time (sec)	8.54	2.37	1.17
Setting time (sec)	16.1	4.49	6.27
Steady state error	0.22	0.09	0.06
Overshoot (OS%)	—	—	17.3

Notes: $0 < \boldsymbol{K_2} < 2.2$ for stability

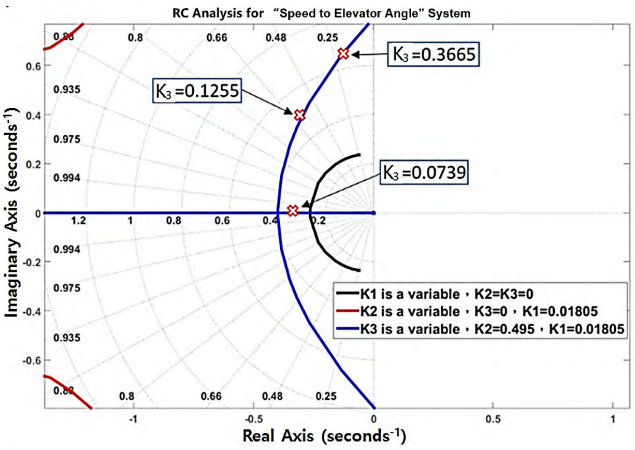

FIGURE 27. RC analysis with $K_1 = 0.01805$, $K_2 = 0.495$, and K_3 is a variable in Eq. (44).

ratio, we chose $\boldsymbol{K_3} = 0.1255$. The step responses based on these three different $\boldsymbol{K_3}$ values are shown in Table 18.

By comparing the system performances of the different $\boldsymbol{K_3}$ values, we can find that when $\boldsymbol{K_3} = \mathbf{0.1255}$, as the whole, the system will have a more reasonable, suitable response for UAV. Therefore, in this paper, the new design PID controller for transfer function from the elevator angle

TABLE 18. $K_1 = 0.01805$, $K_2 = 0.495$, and K_3 is a variable.

Characteristic	$K_3 = 0.0739$	$K_3 = 0.1255$	$K_3 = 0.3665$
Peak time (sec)	—	11.3	5.72
Rise time (sec)	11.2	5.03	1.83
Setting time (sec)	21.3	14	34.9
Steady state error	0	0	0
Overshoot (OS%)	—	3.27	57.6

Notes: $0 < \boldsymbol{K_3} < 0.56$ for stability

to speed is represented as $\boldsymbol{C_7(s)}$ (shown in Eq. (45)). This method of "Reverse Gain PID Controller" is very useful for designers to help overcome the negative effects of the non-minimum phase system that the Ziegler–Nichols method or other controllers can't handle.

$$\boldsymbol{C_7}(\boldsymbol{s}) = \frac{-\mathbf{0.01805} * (\boldsymbol{s}^2 + \mathbf{0.495}\boldsymbol{s} + \mathbf{0.1255})}{\boldsymbol{s}} \quad (45)$$

After the "Reverse Gain PID Controller" compensates for the "elevator angle to speed" system, we believe that this originally unstable non-minimum phase system has already been modified to a stable system. However, based on personal past experiences, a perfect controller design must consider many design aspects, especially about the coupling influences among the controller parameters, poles, and zeros. It is important that not all systems are the same. Therefore, even though we have created a new method or technique, it is impossible to suit all different systems and yield them to the perfectly desired responses at once. Thence, after having finished designing the controller, it is necessary to analyze if there are any derivative coupling effects between the newly designed controller and the original unique system. For example, it is certain that Eq. (45) is already a very nice solution for the non-minimum phase systems. However, noticing Eq. (45) which is specially designed for the "elevator angle to speed" system (shown in FIGURE 13), we can find that Eq. (45) contains a pair complex-conjugate zeros: $-0.25 \pm 0.25i$. The pole-zero distribution of open-loop transfer function in FIGURE 13 with Eq. (45) is represented as Eq. (46):

$$\begin{cases} \boldsymbol{zeros}: -\mathbf{228}, \mathbf{5.05}, -\mathbf{0.25} \pm \mathbf{0.25}\boldsymbol{i} \\ \boldsymbol{poles}: -\mathbf{14.25} \pm \mathbf{8.71}\boldsymbol{i}, -\mathbf{1.95} \pm \mathbf{0.87}\boldsymbol{i}, \\ \quad -\mathbf{0.336} \pm \mathbf{0.31}\boldsymbol{i} \end{cases} \quad (46)$$

There will be a big overshoot when a pair complex- conjugate zeros that are close to the jw-axis coincide with the pair complex-conjugate poles which are also near the jw-axis. For this reason about coupling influences above, we should slightly adjust the parameters in Eq. (45).

We repeated the procedures of the "Reverse Gain PID Controller". Firstly, we still retained $\boldsymbol{K_1} = \mathbf{0.01805}$ as a good

TABLE 19. Closed-loop responses based on the transfer function of "elevator angle to speed" system.

Characteristic	Original system [12]	$\mathbf{C_7(s)}$
Peak time (sec)	System is divergent	2.17
Rise time (sec)	System is divergent	0.631
Setting time (sec)	System is divergent	11.4
Steady state error	System is divergent	0
Overshoot (OS%)	System is divergent	31.8

TABLE 20. Closed-loop responses based on the transfer function of "elevator angle to speed" system.

Characteristic	Original System	New Designed
Controller	—	$\mathbf{C_8(s)}$
Peak time (sec)	System is divergent	0.781
Rise time (sec)	System is divergent	1.25
Setting time (sec)	System is divergent	6.98
Steady state error	System is divergent	0
Overshoot (OS%)	System is divergent	7.24

foundation of Eq. (45) and yielded the unstable root trajectories in RHS to the LHS of s-plane. Secondly, we should not generate another complex-conjugate zeros close to jw-axis to avoid producing too large overshoot. Therefore, we changed from $\boldsymbol{K_2} = 0.495$ to $\boldsymbol{K_2} = 0.184$. We also adjusted from $\boldsymbol{K_3} = 0.1255$ to $\boldsymbol{K_3} = 0.0639$. Therefore, the new transfer function of the new "Reverse Gain PID Controller" was altered to $\boldsymbol{C_8(s)}$ (shown in Eq. (47)).

$$\boldsymbol{C_8}(\boldsymbol{s}) = \frac{-\mathbf{0.01805} * (\boldsymbol{s^2} + \mathbf{0.184}\boldsymbol{s} + \mathbf{0.0739})}{\boldsymbol{s}} \quad (47)$$

The pole-zero distribution of open-loop transfer function in FIGURE 13 with new controller $\boldsymbol{C_8(s)}$ is also shown as Eq. (48):

$$\begin{cases} \boldsymbol{zeros} : -\mathbf{5.152}, \mathbf{0.1519} \\ \boldsymbol{poles} : -\mathbf{10}, -\mathbf{0.0618} \pm \mathbf{0.2359}\boldsymbol{i}, \\ \quad -\mathbf{11.4682} \pm \mathbf{7.2882}\boldsymbol{i} \end{cases} \quad (48)$$

From Eq. (48), it is obvious that there are no complex-conjugate zeros close to jw-axis to stimulate the overshoot. We believe that the new "Reverse Gain PID Controller" (shown in Eq. (47)) will perform better than origin one (shown in Eq. (45)).

Table 19 is the response comparison between the original system [12] and our original "Reverse Gain PID Controller" ($\boldsymbol{C_7}(\boldsymbol{s})$). Table 20 is also the response comparison between the original system [12] and our new "Reverse Gain PID Controller" ($\boldsymbol{C_8}(\boldsymbol{s})$). Besides, FIGURE 28 shows the closed response of the "elevator angle to speed" system with our new "Reverse Gain PID Controller" $\boldsymbol{C_8(s)}$.

For the non-minimum phase system (i.e. "elevator angle to speed" system in this paper) we have created the "Reverse Gain PID Controller" to handle it (shown in Eq. (44) and Eq. (45)). From Table 19, we can find that the originally unstable non-minimum phase has already been corrected. We created a new controller to correct the unstable system that the author can't solve in [12]. Moreover, as we indicated and estimated above, a perfect controller design must consider the coupling influences among the controller parameters, poles, and zeros. In Table 19, the closed-loop responses of the "elevator angle to speed" system with "Reverse Gain PID Controller" $\boldsymbol{C_7(s)}$ are really good except

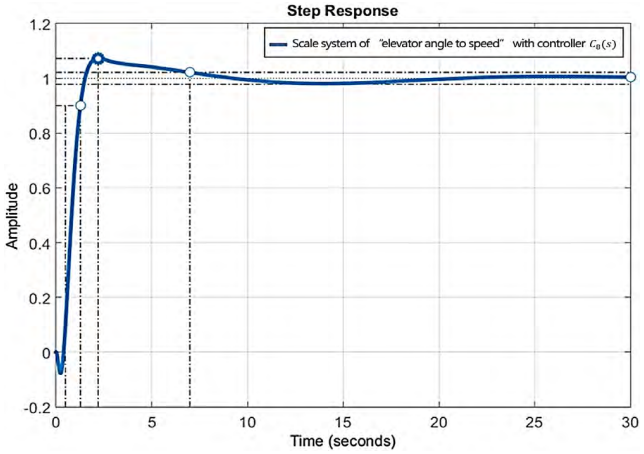

FIGURE 28. Closed response of "elevator angle to speed" system with controller $C_8(s)$.

for the big overshoot due to the coupling effects among the complex-conjugate poles and zeros near the jw-axis. Also, the closed-loop responses of the "elevator angle to speed" system with our new "Reverse Gain PID Controller" $\boldsymbol{C_8(s)}$ seems perfect, and it has already fixed the drawback of the big overshoot in Table 19. From Table 19, Table 20, and FIGURE 28, we can find that the "Reverse Gain PID Controller" which we created helps to overcome the negative effect from non-minimum phase, and it surely stabilizes the divergent "elevator angle to speed" system. In addition, the new method in this research is both academic and efficient. It makes it good reference material that can be applied by researchers in their follow-up research.

After completing the "Reverse Gain PID Controller" to successfully improve the unstable non-minimum phase system, we would like to further explain the significance of this experiment.

In addition, from the mathematical models deduced and the contents of [12] in this study, we can clearly see that the scaled UAV Scale Cessna 182 with a 1:6.65 scale reduction ratio for the Cessna 182 has a zero on the right-hand-side of the s-plane in its original "elevator angle to speed" system, so it is true that a non-minimum phase system is correct.

For aircraft and satellite systems, the non-minimum phase system is not a rare situation, and because the non-minimum phase system is likely to cause internal instability of the vehicle system, the controller design of the flight vehicle quite similar difficulties, and most of the operators can only improve the responses of the system by changing the design of the vehicle or adding bias damper and other hardware modifications, and because of this, C.-Y. Yang, when designing the controller on all the subsystems of Scale Cessna 182, stated that [12], for the unstable output state of the ''elevator angle to speed'' system, if the method of the controller design is used to improve the response system, he cannot do anything. Because of this, we will develop the ''Reverse Gain PID Controller'' to improve the system in this paper.

Also, due to the different designs and functions of the vehicle, other subsystems of the aircraft may also have the characteristics of non-minimum phase systems. Therefore, what we want to emphasize in this paper is that the new ''Reverse Gain PID Controller'' of this research has greatly improved the ability of non-minimum phase systems.

Thus, whether or not this non-minimum phase system is present in the longitudinal motion of the UAV or in a particular subsystem of the lateral motion, we can apply the ''Reverse Gain PID Controller'' to improve the response and robustness of the system. Even if other non-minimum-phase systems of power carriers are deficient, we believe that the ''Reverse Gain PID Controller'' can also be a great help. This is the discussing point and contribution we have always wanted to emphasize in this paper.

Ultimately, the new method in this research is both academic and efficient. It makes good reference material that can be applied by researchers in their follow-up research.

3) ''Elevator angle to pitch angle'' system

According to the mathematical model in [12], the block diagram for ''elevator angle to pitch angle'' system is shown in FIGURE 29:

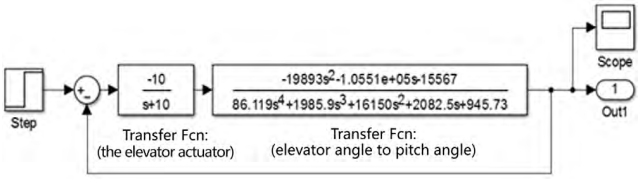

FIGURE 29. Block diagram of ''elevator angle to pitch angle'' system.

The original controller designed in [12] appling the Ziegler PID method. The PID parameters are $\boldsymbol{K_p} = \mathbf{1.2}$, $\boldsymbol{K_i} = \mathbf{2.1347}$,and $\boldsymbol{K_d} = \mathbf{0.11}$, respectively. The controller transfer function can be represented in the form as shown in Eq. (49):

$$\boldsymbol{C_9}(\boldsymbol{s}) = \frac{\mathbf{0.11} * (\boldsymbol{s^2} + \mathbf{10.9}\boldsymbol{s} + \mathbf{19.4})}{\boldsymbol{s}} \tag{49}$$

Before we improve the original design, we analyzed the ''elevator angle to pitch angle'' system in FIGURE 29. The pole-zero distribution for open-loop transfer function is shown as follows:

$$\begin{cases} \boldsymbol{zeros} : \mathbf{-5.152}, \mathbf{-0.1519} \\ \boldsymbol{poles} : \mathbf{-10}, \mathbf{-0.0618 \pm 0.2359}\boldsymbol{i}, \\ \quad \mathbf{-11.4682 \pm 7.2882}\boldsymbol{i} \end{cases} \tag{50}$$

From the Eq. (50), it can be found that there is a pair of complex-conjugate poles very close to the imaginaries axis. These complex-conjugate poles will result in the large overshoot and long setting time. Sometimes, the external disturbance will excite these complex-conjugate poles to yield to the instability. Thus, to eliminate the negative effects from the complex-conjugate poles, in this case, we decided to design the Notch filter to cancel the complex-conjugate poles above and improve the response of the system.

The transfer function of the Notch filter is shown as Eq. (51), where $\boldsymbol{a}$ and $\bar{a}$ are the complex-conjugate poles we want to delete; $\boldsymbol{b}$ and $\boldsymbol{c}$ are the kinds of the desired poles or the ones that have been designed to eliminate the unfavorable zeros in the original system. In Eq. (51), we set $\boldsymbol{a}$ and $\bar{a}$ as $\mathbf{-0.0618 \pm 0.2359}\boldsymbol{i}$, and $\boldsymbol{b} = \mathbf{0.1519}$, then we applied the RC criterion to get $\boldsymbol{c} = \mathbf{0.1}$. Finally, based on RC criterion, we can get the controller gain $\boldsymbol{K} = 0.74$. The complete Notch filter equation is shown as Eq. (52):

$$\boldsymbol{G_{10}}(\boldsymbol{s}) = \frac{\boldsymbol{s^2} + \boldsymbol{K_1 s} + \boldsymbol{K_2}}{\boldsymbol{s^2} + \boldsymbol{K_3 s} + \boldsymbol{K_4}} = \frac{\boldsymbol{K} * (\boldsymbol{s} + \boldsymbol{a})\,(\boldsymbol{s} + \bar{a})}{(\boldsymbol{s} + \boldsymbol{b})\,(\boldsymbol{s} + \boldsymbol{c})} \tag{51}$$

$$\boldsymbol{G_{10}}(\boldsymbol{s}) = \frac{\mathbf{0.74}(\boldsymbol{s} + \mathbf{0.0618} + \mathbf{0.2359}\boldsymbol{i})(\boldsymbol{s} + \mathbf{0.0618} - \mathbf{0.2359}\boldsymbol{i})}{(\boldsymbol{s} + \mathbf{0.159})\,(\boldsymbol{s} + \mathbf{0.1})} \tag{52}$$

Cascading Eq. (52) before the ''elevator angle to pitch angle'' system in FIGURE 29 and applying the Matlab/Simulink, we can get the step response of the closed-loop system for ''elevator angle to pitch angle'' system with Notch filter (shown in FIGURE 30). Besides, the step response specifications of the closed-loop system for ''elevator angle to pitch angle'' system are also shown in Table 21.

TABLE 21. Step response specifications of the closed-loop system for ''elevator angle to pitch angle'' system.

Characteristic	Original System	Original PID Controller [12]	Notch-filter
Controller	–	$\boldsymbol{C_9(s)}$	$\boldsymbol{C_{10}(s)}$
Peak time (sec)	0.352	0.6007	0.409
Rise time (sec)	0.148	0.11	0.209
Setting time (sec)	27.5	1.5207	0.88
Steady state error	7.6	0	0
Overshoot (OS%)	22.5	9.9562	2.65

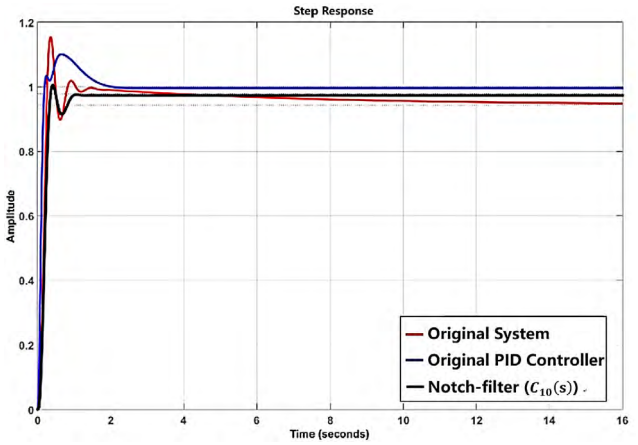

FIGURE 30. Step response of the closed-loop system for "elevator angle to pitch angle" system (Original system), Original PID controller, and Notch-filter ($C_{10}(s)$).

From FIGURE 30 and Table 22, it is obvious that Notch filter not only eliminates the negative effects from the complex-conjugate poles in original "elevator angle to pitch angle" system but also improves the response of the system, and especially, reduces most of the overshoot that the UAV in particular needs to avoid.

4) "Rudder angle to sideslip angle" system

The mathematical model of the "rudder angle to sideslip angle" system for Scale Cessna 182 is shown as FIGURE 31 [12]:

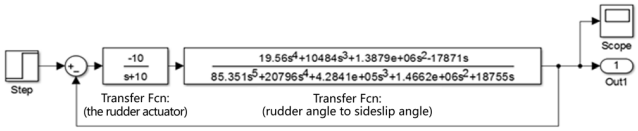

FIGURE 31. Block diagram of "rudder angle to sideslip angle" system.

Yang [12] applied the Ziegler-Nichols method to design the PID controller. The controller parameters are $\boldsymbol{K_p = 0.8}$, $\boldsymbol{K_i = 0.000999}$, and $\boldsymbol{K_d = 0}$, respectively. The PID transfer function can be represented in the form as shown in Eq. (49), and the step response of the closed-loop system is also shown in Table 22:

$$\boldsymbol{C_{11}(s) = \frac{0.2 * (s^2 + 4s + 0.05)}{s}} \tag{53}$$

From Table 22, it is very clear that the transient response in the original "rudder angle to sideslip angle" system is very terrible. There is a long setting time and a very large overshoot in this non-minimum phase system. Even through through the PID compensation (Eq. (53)) [12], in Table 22, we can still find the same problems in the "rudder angle to sideslip angle" system.

Again, before improving the original design, we should first analyze the "rudder angle to sideslip angle" system. In FIGURE 31, the pole-zero distribution for "rudder angle to sideslip angle" system is shown as the Eq. (54):

TABLE 22. Step response specifications of the closed-loop system for "rudder angle to sideslip angle" system.

Characteristic	Original System	Initial Designed in reference [12]
Controller	–	$\boldsymbol{C_{11}(s)}$
Peak time(sec)	17.864	–
Rise time (sec)	0.36	59.48
Setting time (sec)	97.9641	163.88
Steady state error	0.5121	0
Overshoot (OS%)	600.815	189.9

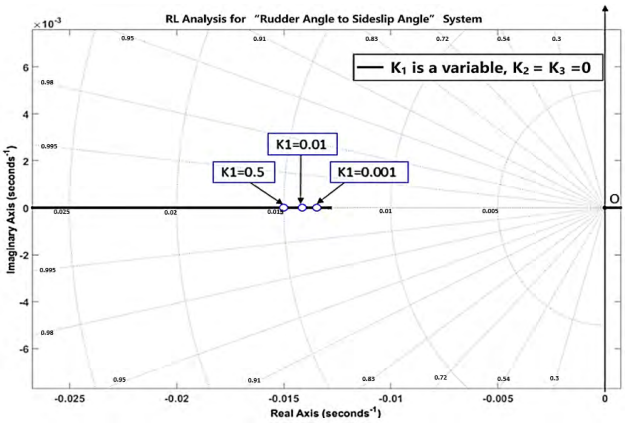

FIGURE 32. RL analysis for "rudder angle to sideslip angle" system, where $K_2 = K_3 = 0$, and K_1 is a variable.

$$\begin{cases} \textit{zero} : \mathbf{0.0129}, \mathbf{-297.3428}, \mathbf{-238.6609} \\ \textit{pole} : \mathbf{-0.0128}, \mathbf{-4.2896}, \mathbf{-10}, \\ \quad \mathbf{-18.0261}, \mathbf{-221.3221} \end{cases} \tag{54}$$

From Eq. (54), we can find that there is a positive zero: 0.0129 in the "rudder angle to sideslip angle" system. The unstable zero (0.0129) with a very small pole (−0.0128) result in very a long setting time and an awfully large overshoot. After the author compensated for the system with the PID controller based on the Ziegler PID method, the fixed system is still worse, and the responses can't satisfy the users. Therefore, in this research, we applied the RC criterion combined with our creativity, "Reverse Gain PID Controller", to effectively improve the worse system.

The transfer function of the "Reverse Gain PID Controller" is shown as Eq. (44) above. According to the design procedures of the controller mentioned above, the first step is to set $\boldsymbol{K_2 = K_3 = 0}$, and $\boldsymbol{K_1}$ as a variable, then to draw the root locus (shown in FIGURE 32). From the RL criterion, we can get the stable range of $\boldsymbol{K_1}$: $\boldsymbol{0 < K_1 < 82}$. We, randomly, selected three stable parameters to be candidates for variable $\boldsymbol{K_1}$, such as 0.5, 0.01, and 0.001. And the step responses of these three different $\boldsymbol{K_1}$ values are also shown in Table 23.

TABLE 23. Step responses of three different K_1.

Characteristic	$K_1 = 0.001$	$K_1 = 0.01$	$K_1 = 0.5$
Peak time (sec)	0.216	0.211	0.143
Rise time (sec)	0	0	0
Setting time (sec)	1.16	1.2	8.8809
Steady state error	1	1	1

Notes: $K_2 = K_3 = 0$

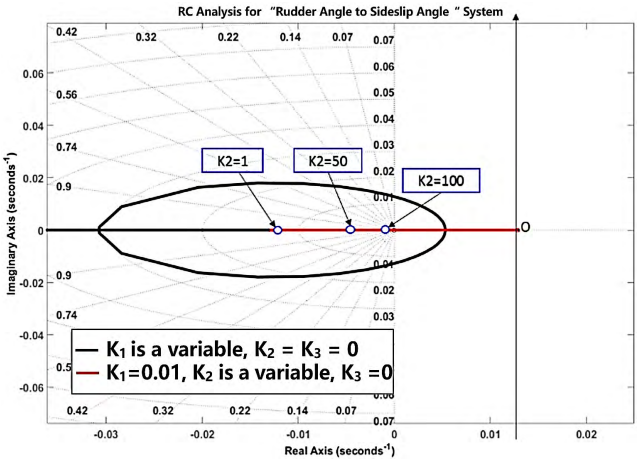

FIGURE 33. RC analysis for "rudder angle to sideslip angle" system, where $K_3 = 0$, $K_1 = 0.01$, and K_2 is a variable.

In FIGURE 32 and Table 23, we see that even though $K_1 = 0.01$ has the similar response to the damping ratio of the system, it is close to $K_1 = 0.001$. However, the location of the characteristic root based on $K_1 = 0.001$ is more left than the $K_1 = 0.001$ one. Additionally, the damping ratio of the characteristic root based on $K_1 = 0.01$ is close to 0.707. This situation will yield to a better transient response. In view of these two reasons, we choose $K_1 = 0.01$.

The second step of the controller design is to set $K_3 = 0$ and $K_1 = 0.01$ which we selected in the first step, and K_2 is a variable. The RC with variable K_2 is shown in FIGURE 33. According to RC criterion, we can also find the stable range: $0 < K_2 < 104$. In FIGURE 33, we arbitrarily picked three stable points i.e. 1, 50, and 100 as the candidates of the variable K_2. The step responses of these three acceptable K_2 values are also shown in Table 24. After integrating the system performances of the different K_2 values, we finally select $K_2 = 1$.

In the third step, we let K_3 be the variable, and $K_2 = 1$, $K_1 = 0.01$ are the fixed constants selected in the first and second steps above. The RC based on this setting can be obtained and shown in FIGURE 33. The stable range K_3 is between 0 and 955. Again, we arbitrarily picked three acceptably stable parameters. They are 70, 130, and 270,

TABLE 24. Step responses from different K_2.

Characteristic	$K_2 = 1$	$K_2 = 50$	$K_2 = 100$
Peak time (sec)	—	—	—
Rise time (sec)	174	483	7100
Setting time (sec)	312	861	12700
Steady state error	1.01	1.91	21.2
Overshoot (OS%)	—	—	—

Notes: $K_3 = 0, K_1 = 0.01$, $0 < K_2 < 104$

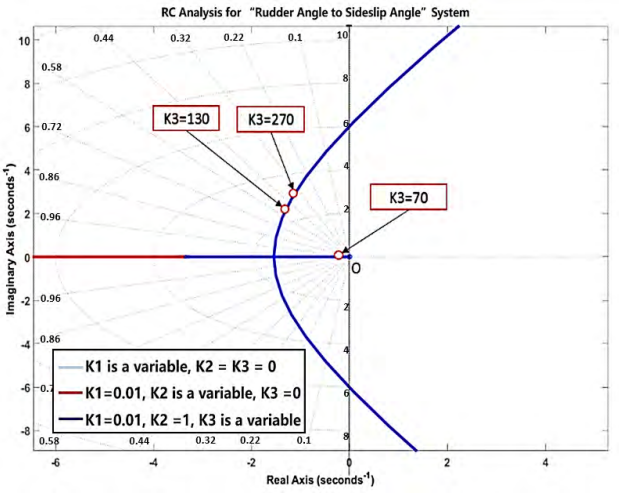

FIGURE 34. RC analysis for "rudder angle to sideslip angle" system, where K_3 is a variable, K_1 and K_2 are fixed constants.

TABLE 25. Step responses from different K_3.

Characteristic	$K_3 = 70$	$K_3 = 130$	$K_3 = 270$
Peak time (sec)	7.6816	2.2709	1.3
Rise time (sec)	2.7263	1.0957	0.5281
Setting time (sec)	4.07	3.03	3.1
Steady state error	0.05	0.023	0.01
Overshoot (OS%)	—	1.8231	24.0468

Notes: $K_2 = 1, K_1 = 0.01$

respectively. The step responses based on these three different K_3 values are also shown in Table 25.

Upon summarizing the system performance of different K_3 values in Table 25, we finally chose 130 as K_3 value. The controller designed to improve the "rudder angle to sideslip angle" system is shown as Eq. (55).

$$C_{12}(s) = \frac{-0.01 * (s^2 + s + 130)}{s} \tag{55}$$

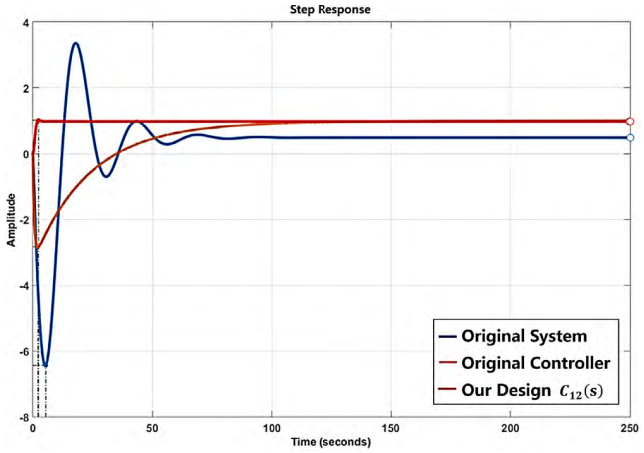

FIGURE 35. Step response of the closed-loop system for "rudder angle to sideslip angle" system (Original System), cascading $C_{11}(s)$ (Original controller), and cascading Our Design $C_{12}(s)$.

TABLE 26. Step response specifications of the closed-loop system for "rudder angle to sideslip angle" system.

Characteristic	Original System	Original Controller	Our Design
Controller	—	$C_{11}(s)$	$C_{12}(s)$
Peak time (sec)	17.864	—	2.2844
Rise time (sec)	0.36	59.48	1.134
Setting time (sec)	97.964	163.88	2.99
Steady state error	0.5121	0	0
Overshoot (OS%)	600.815	189.9	1.4872

After cascading Eq. (55) before the "rudder angle to sideslip angle" system in FIGURE 31 and applying the Matlab/Simulink, we can get the step response of the closed-loop system for "rudder angle to sideslip angle" system with our designed controller $\boldsymbol{C_{12}(s)}$ (shown in FIGURE 35). Furthermore, step response specifications of the closed-loop system for "rudder angle to sideslip angle" system is also shown in Table 26.

After summarizing the system performances in FIGURE 35 and Table 26, it's very clear that our design controller $\boldsymbol{C_{12}(s)}$ helps to solve the non-minimum phase, "rudder angle to sideslip angle" system, and effectively improves both the transient response and steady-state error, simultaneously. Likewise, there has always been a problem, i.e. the coupling negative relation between the reverse response and the setting time. We all know if a non-minimum phase has an unstable zero, the big reverse response comes with a smaller setting time. In contrast, in a normal situation, when the designers try to reduce the reverse response, they will get a longer setting time. Hence, designers really face difficult decisions. This situation can be also shown in FIGURE 35 and Table 26. However, our designed controller $\boldsymbol{C_{12}(s)}$ effectively and

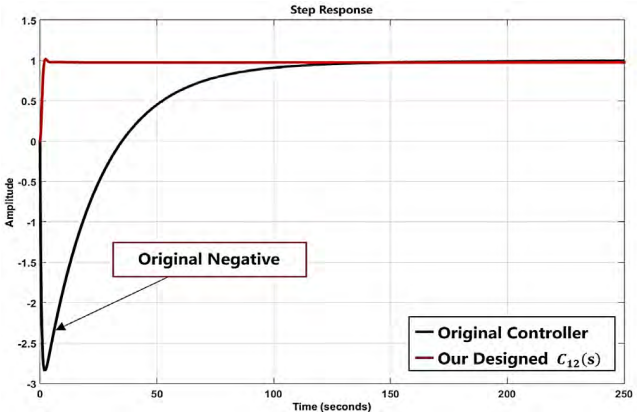

FIGURE 36. Our designed controller $C_{12}(s)$ effectively and completely improves the dilemma of the non-minimum phase system.

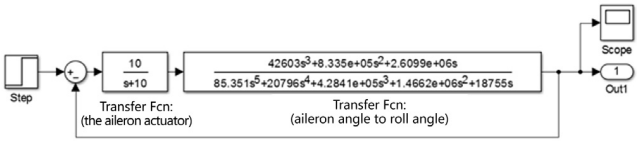

FIGURE 37. Block diagram of "aileron angle to roll angle" system.

completely improves this dilemma (shown in FIGURE 35, FIGURE 36, and Table 26). For this reason, the method for controller design mentioned in this research is a very nice solution to the problem which designers encounter and should definitely be referred to by researchers who wish to conduct relevant research on this subject.

5) "Aileron angle to roll angle" system

The mathematical model of the "aileron angle to roll angle" system for Scale Cessna 182 is shown as FIGURE 37 [12]:

The original PID parameters in [12] are $\boldsymbol{K_p = 1.2}$, $\boldsymbol{K_i = 2.1347}$, and $\boldsymbol{K_d = 0.11}$, respectively. And the controller transfer function can be represented in the form as shown in Eq. (49):

$$\boldsymbol{C_{13}(s) = \frac{3.6 * (s^2 + 5.28s + 69.4)}{s}} \tag{56}$$

Table 27 represents the closed-loop responses of the original "aileron angle to roll angle" system and the "aileron angle to roll angle" system after cascading the controller $\boldsymbol{C_{13}(s)}$.

According to Table 27, the steady-state error of the original "aileron angle to roll angle" system is good enough. However, the setting time is long. After the author designed a controller $\boldsymbol{C_{13}(s)}$, the setting time became acceptable, but the overshoot seemed to become a little large. In view of this, we decided to design a phase lead-lag compensator to improve both the transient response and steady-state error of the original system. Moreover, this phase lead-lag compensator will also improve both the overshoot and the setting time of the corrected system of which the author cascaded

TABLE 27. The step response specifications for "aileron angle to roll angle" system.

Characteristic	Original System	Original Controller
Controller	—	$C_{13}(s)$
Peak time (sec)	—	0.0393
Rise time (sec)	1.0751	0.0217
Setting time (sec)	2.1546	0.7787
Steady state error	0.0071	0
Overshoot (OS%)	0.7135	19.641

the controller $C_{13}(s)$ with the original "aileron angle to roll angle" system.

Before we design the controller, we always first analyze the original system. After doing this work, we will be more capable to design a suitable controller to match our system. According to FIGURE 37 [12], the pole-zero distribution for open-loop transfer function is shown as follows:

$$\begin{cases} zero : 0, -3.9145, -15.65 \\ pole : 0, -0.0128, -4.2896, \\ \quad -10, -18.0261, -221.3221 \end{cases} \tag{57}$$

From the Eq. (57) we can find that phase lead-lag compensator is certainly a good choice to improve the system. The transfer function of the phase-lead compensator is shown as Eq. (58), where K is the compensator gain, while $-z_1$ and $-z_2$ are the compensator zeroes that are designed to delete the poor poles of the original system. $-p_1$ and $-p_2$ are the compensator poles that we want. Therefore, the designed phase lead-lag compensator is shown as Eq. (59) that can delete the poor poles: -0.0128, -4.2896 of the original "aileron angle to roll angle" system.

$$C_{14}(s) = \frac{K * (s + z_1)(s + z_2)}{(s + p_1)(s + p_2)} \tag{58}$$

$$C_{14}(s) = \frac{3.08 * (s + 4.29)(s + 0.0128)}{(s + 4.58)(s + 0.01)} \tag{59}$$

Upon cascading Eq. (59) before the "aileron angle to roll angle" system in FIGURE 37 and applying the Matlab/Simulink, we can get the step response of the closed-loop system for "aileron angle to roll angle" with the phase lead-lag compensator (shown in FIGURE 38 and Table 28).

From FIGURE 38 and Table 28, it is obvious that the phase-lead compensator undoubtedly improves the system response of the system, especially in regards of time setting and overshoot.

6) "Rudder angle to yaw angle" system

The mathematical model of the "rudder angle to yaw angle" system for Scale Cessna 182 is shown in FIGURE 39 [12]:

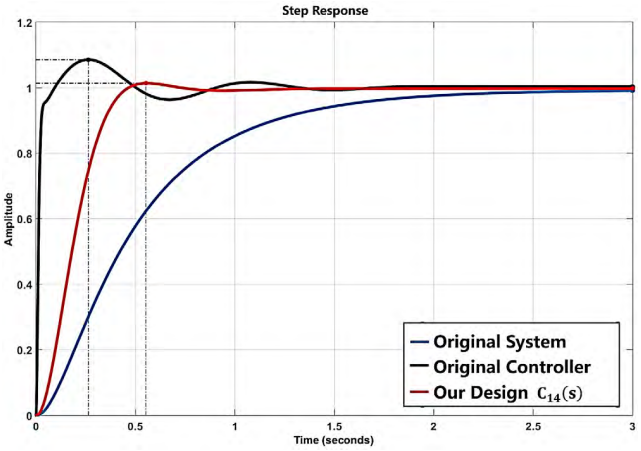

FIGURE 38. Step response of the closed-loop system for "aileron angle to roll angle" system (Original System), cascading $C_{13}(s)$ (Original controller), and cascading Our Design $C_{14}(s)$.

TABLE 28. Step response specifications of the closed-loop system for "aileron angle to roll angle" system.

Characteristic	Original System	Original Controller	Our Design
Controller	—	$C_{13}(s)$	$C_{14}(s)$
Peak time (sec)	—	0.0393	1.013
Rise time (sec)	1.0751	0.0217	0.2765
Setting time (sec)	2.1546	0.7787	0.4212
Steady state error	0.0071	0	0.002
Overshoot (OS%)	0.7135	19.641	1.519

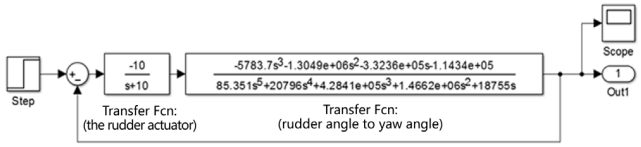

FIGURE 39. Block diagram of "rudder angle to yaw angle" system.

According to FIGURE 39 [12], the pole-zero distribution for open-loop transfer function is shown as Eq. (60):

$$\begin{cases} zero : 0, -3.9145, -15.65 \\ pole : 0, -0.0128, -4.2896, \\ \quad -10, -18.0261, -221.3221 \end{cases} \tag{60}$$

In FIGURE 39, drawing the RL based on the "rudder angle to yaw angle" system, it is obvious that there are two root trajectories toward to the RHS of the s-plane (shown in FIGURE 40). Also, since the "rudder angle to yaw angle" system is system type "1", we should try hard not to design the PI or PID to avoid increasing the superfluous pole located at its origin.

The authors tried to design the controller $C_{15}(s)$ to improve the "rudder angle to yaw angle" system of the Scale

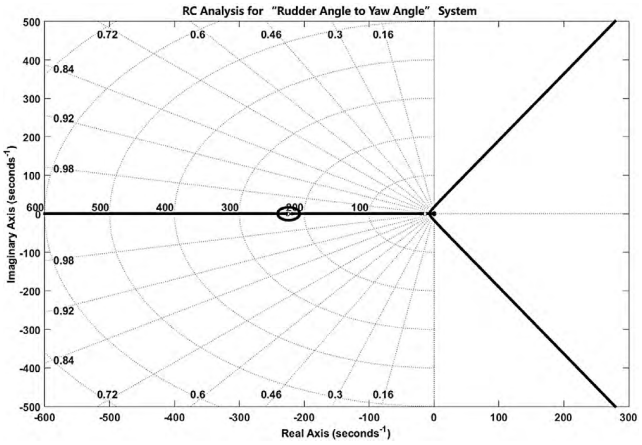

FIGURE 40. RL analysis for "rudder angle to yaw angle" system.

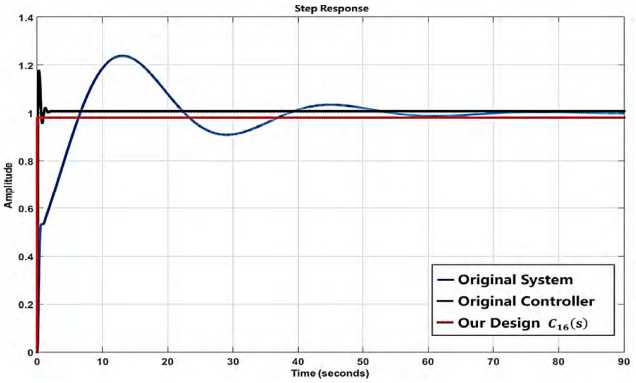

FIGURE 41. Step response of the closed-loop system for the "rudder angle to yaw angle" system (Original System), cascading $C_{15}(s)$ (Original controller), and cascading Our Design $C_{16}(s)$.

TABLE 29. Step response specifications of the closed-loop system for "rudder angle to yaw angle" system.

Characteristic	Original System	Original Controller	Our Designed
Controller	—	$\mathbf{C_{15}(s)}$	$\mathbf{C_{16}(s)}$
Peak time (sec)	1.31	0.201	—
Rise time (sec)	5.21	0.0853	0.00343
Setting time (sec)	50.2	0.8866	0.0102
Steady state error	0	0	0
Overshoot (OS%)	23.9	22.7891	—

Cessna 182. Their original PID parameters in [12] are $\boldsymbol{K_p} = \mathbf{5}$, $\boldsymbol{K_i} = \mathbf{40}$, and $\boldsymbol{K_d} = \mathbf{0.6}$, respectively, and this controller transfer function can be represented in the form as Eq. (49):

$$\boldsymbol{C_{15}}(\boldsymbol{s}) = \frac{\mathbf{0.6} * (\boldsymbol{s^2} + \mathbf{8.33}\boldsymbol{s} + \mathbf{66.67})}{\boldsymbol{s}} \tag{61}$$

The controller $\boldsymbol{C_{15}}(\boldsymbol{s})$ above is not very suitable. In this research, we redesigned the controller for the "rudder angle to yaw angle" system. To avoid increasing the surplus pole located at its origin, we decided to design a controller which consists of a pair of complex-conjugate zeros. This controller mode is not a part of the current controller category. However, it doesn't matter if a controller can improve the system or not; thus it is a nice controller. In this research, we call this controller "complex-conjugate zeros controller".

The transfer function of our new mode controller, "complex-conjugate zeros controller", is shown as Eq. (62). Where $\boldsymbol{K}$ is the system gain, and $\boldsymbol{K_1}$, $\boldsymbol{K_2}$ are the constants. We applied the RC criterion to obtain the values of the $\boldsymbol{K_1}$ and $\boldsymbol{K_2}$. The design steps are the same as the procedures of the above section IVA1 in this research, so we get $\boldsymbol{K_1} = \mathbf{17.5}$, $\boldsymbol{K_2} = \mathbf{76.8}$. Additionally, based on the RC criterion, we can also get the system gain $\boldsymbol{K} = \mathbf{1}$. Therefore, our new mode controller $\boldsymbol{C_{16}}(\boldsymbol{s})$ is represented as Eq. (63):

$$\boldsymbol{C_{16}}(\boldsymbol{s}) = \boldsymbol{K} * (\boldsymbol{s^2} + \boldsymbol{K_1 s} + \boldsymbol{K_2}) \tag{62}$$

$$\boldsymbol{C_{16}}(\boldsymbol{s}) = \boldsymbol{s^2} + \mathbf{17.5}\boldsymbol{s} + \mathbf{76.8} \tag{63}$$

When cascading Eq. (63) before the "rudder angle to yaw angle" system in FIGURE 39 and applying the Matlab/Simulink, we can get the step response of the closed-loop system for "rudder angle to yaw angle" system with the new mode controller $\boldsymbol{C_{16}}(\boldsymbol{s})$ (shown in FIGURE 41). Also, the step response specifications of the closed-loop system for "rudder angle to yaw angle" system are also shown in Table 29.

From the FIGURE 41 and Table 29, we can clearly see the new mode controller $\boldsymbol{C_{16}}(\boldsymbol{s})$ does improve both the setting time and overshoot of the system. This design is really much better compared to the other design in [12]. Besides, from the different designs among the section, we can come to the conclusion that since different systems have various types of pole-zero distributions, the special types of systems should match their proper controllers to improve the system's performance. Therefore, for a good controller designer, the thinking and design methods must be creative and flexible.

B. CORRECTION INSTRUCTION FOR ERROR TRANSFER FUNCTIONS

From section IVA1 to section IVA6, after we designed the various controllers to solve the problems of the different subsystems for scale Cessna 182, in the accidental situation, we found that, based on our knowledge, the transfer functions of the 6 original subsystems in [12] are a little strange. Then we ourselves tried to establish mathematical model including 6 subsystems and checked every parameter of scale Cessna 182 again. Finally, we found that the system model is all correct except for the gravity value. We found that when the author substituted the real parameters of the scale Cessna 182 in the formulae, he forgot to change the gravity value 9.8 (N / kg) to $\mathbf{32.174}(\boldsymbol{ft}/\boldsymbol{sec^2})$. In view of the aerodynamic dynamics, the designers should use Imperial Units, not Metric Units. Apart from this small mistake, everything else is correct. Therefore, our designs from section IVA1 to section IVA6

are still effective and valid, especially for the systems that have the same system properties. However, in order to avoid controversy, in section IVC, we will redesign the controllers for the 6 true subsystems of the scale Cessna 182. Beside this, in order to enrich the controller designs, we will add the practically relative stability which is the real need for the application of UAV and its task requirements. Hence, we will give more instructions to demonstrate how to improve both the transient responses and steady-state errors while taking relative stability into account at the same time.

Before we start to design the new controller based on relative stability, we thought we had better use an example as a comparison to help us introduce the use of relative stability. In section IVA1, the block diagram of the ''elevator angle to AOA'' system before being corrected is shown in FIGURE 6.

The originally designed PID controller $\boldsymbol{C_1}(\boldsymbol{s})$ in [12] is also represented as Eq. (38) above. According to FIGURE 6, the pole-zero distribution for open-loop transfer function is shown as Eq. (64):

$$\begin{cases} \boldsymbol{zero}: -\mathbf{446.76}, -\mathbf{0.06} \pm \mathbf{0.29}\boldsymbol{i} \\ \boldsymbol{pole}: -\mathbf{10}, -\mathbf{11.47} \pm \mathbf{7.29}\boldsymbol{i}, -\mathbf{0.0618} \pm \mathbf{0.236}\boldsymbol{i} \end{cases} \tag{64}$$

Upon designing the robust controller for the ''elevator angle to AOA'' system, we set the general form of this controller as Eq. (65):

$$\begin{aligned} \boldsymbol{G_{PID}}(\boldsymbol{s}) &= \frac{\boldsymbol{K} * (\boldsymbol{s} - \boldsymbol{z_1})(\boldsymbol{s} - \boldsymbol{z_2})}{(\boldsymbol{s} - \boldsymbol{p_1})} \\ &= \frac{\boldsymbol{K_i} + \boldsymbol{K_p s} + \boldsymbol{K_d s^2}}{\boldsymbol{s}} = \boldsymbol{C_{17}}(\boldsymbol{s}) \end{aligned} \tag{65}$$

where $\boldsymbol{K}$ is the system gain.

According to Eq. (64) and Eq. (65), we find that this situation is suitable to apply the model reduction method for the improvement of the system because reducing the relative degree of the system will yield a better response. Also, apart from the model reduction method, regarding relative stability, it can be obtained by several graphical tools in the frequency domain, such as Nyquist criterion, Bode plot, Nichols plot, and so on. In this research, we apply the Nichols plot and Bode plot to help obtain the relative stability of the UAV. The following is the procedure to design the robust controller.

According to FIGURE 6 and the Eq. (7), we first applied the model reduction method to improve the system.

The first step is to select one pole that we wanted to delete in the ''elevator angle to AOA'' system. Assuming that the unwanted pole $\mathbf{p_{unwanted}} = -10$, therefore, the controller $\mathbf{C_{17}}(\mathbf{s})$ should have a zero located at -10. Also, we wanted to add a pole $\mathbf{p_1}$ located at the origin of the s-plane to improve the steady-state error of the system. Therefore, the controller $\mathbf{C_{17}}$ (s) should contain the term: $\boldsymbol{G_{db}}(\boldsymbol{s}) = \frac{s+10}{s}$.

Secondly, when cascading the $\boldsymbol{G_{db}}(\boldsymbol{s})$ with Eq. (7) and drawing the Nichols plot by Matlab command: ''Nichols'', we can get the Nichols plot for ''elevator angle to AOA'' system as shown in FIGURE 42:

Thirdly, observing the Nichols plot to set up the other zero in Eq. (65), from FIGURE 42, we can find the worst phase of

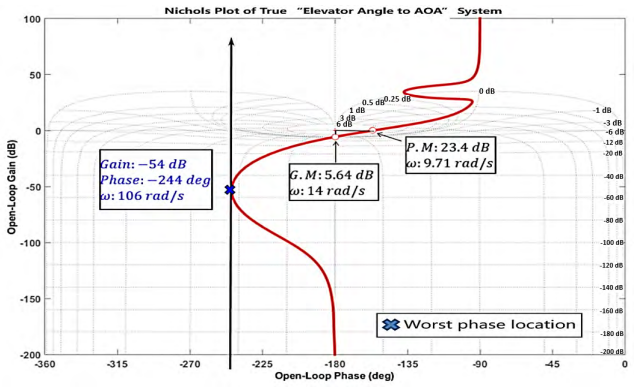

FIGURE 42. Nichols plot of the true "elevator angle to AOA" system with the $G_{db}(s)$.

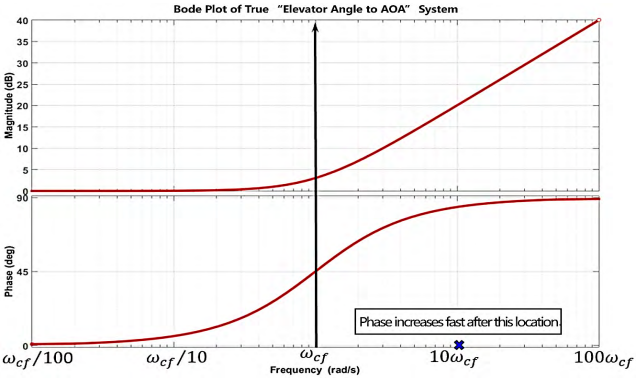

FIGURE 43. Bode plot of the true "elevator angle to AOA" system with the $G_{db}(s)$.

the system happened at frequency $\boldsymbol{\omega} = \mathbf{106}^{\boldsymbol{rad}}/_{\boldsymbol{sec}}$, where the phase is $-\mathbf{244}^{\boldsymbol{o}}$. After we add a zero, the system phase can be pulled high to $\mathbf{90}^{\boldsymbol{o}}$. Assuming that this wanted zero is located at frequency $\boldsymbol{\omega_{cf}}$, according to the criterion of the Nichols plot and our past experiences, if we set $\mathbf{10}\boldsymbol{\omega_{cf}} \cong \boldsymbol{\omega} = \mathbf{106}$, we will boost higher system phase. Beside this, the slope of the frequency $\boldsymbol{\omega_{cf}}$ is positive. This location will not offset the raise phase when we add zero. The phase situation can also be clearly analyzed by Bode plot (shown in FIGURE 43).

Therefore, in order to facilitate the calculation, we set $\boldsymbol{\omega_{cf}} \cong \mathbf{10}^{\boldsymbol{rad}}/_{\boldsymbol{sec}}$, and also choose the other zero of the controller to be -10.

The fourth step is to combine the selected zero from third step with $\boldsymbol{G_{db}}(\boldsymbol{s})$. The result $\boldsymbol{G_{dbz}}(\boldsymbol{s})$ can be represented as Eq. (66):

$$\boldsymbol{G_{dbz}}(\boldsymbol{s}) = \frac{(\boldsymbol{s} + \mathbf{10})(\boldsymbol{s} + \mathbf{10})}{\boldsymbol{s}} \tag{66}$$

After cascading $\boldsymbol{G_{dbz}}(\boldsymbol{s})$ with the ''elevator angle to AOA'' system, the system G.M. becomes ∞, P.M. becomes $\mathbf{33.8}^{\boldsymbol{o}}$ (shown in FIGURE 44), and $\boldsymbol{G_{dbz}}(\boldsymbol{s})$ does contribute $\mathbf{90}^{\boldsymbol{o}}$ on the worst phase location. However, $\mathbf{33.8}^{\boldsymbol{o}}$ is not enough for UAV relative stability. For the sake of safety, according to the US military standard (MIL-F-9490D) [16], the flight carrier has to be more than 6dB on gain margin (G.M.). In addition,

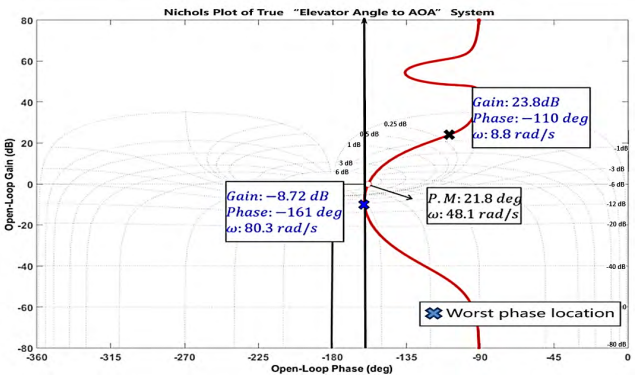

FIGURE 44. Nichols plot for the open-loop transfer function of the "elevator angle to AOA" system with the controller $C_{dbz}(s)$.

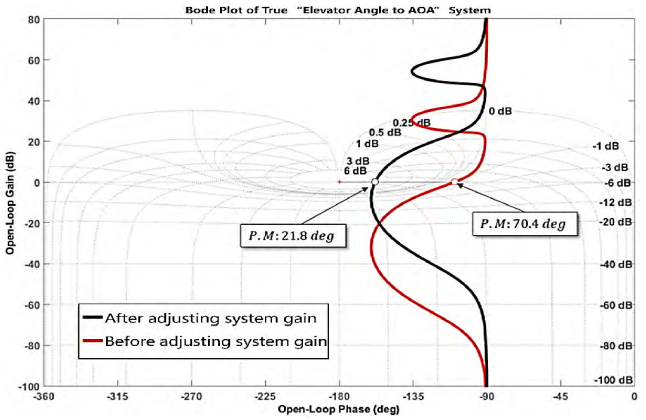

FIGURE 45. The comparisons of the Nichols plot for those with or without the gain K.

after losing verification of the system, the relative stability of the whole carrier system must be above 4.5dB. The P.M. is better than $\mathbf{60}^{o}$.

Since the P.M. is not enough, we decided to improve the P.M. to $\mathbf{70}^{o}$. Therefore, we have to yield the frequency $\boldsymbol{\omega}$ to cross over the $\mathbf{0}dB$ line. The desired position is located at $(-\mathbf{110}^{o}, \mathbf{23.8}dB)$. Hence, the fifth step of the controller design is to provide a suitable system gain $\boldsymbol{K}$ to improve the P.M. In order to cross over the $\mathbf{0}dB$ line, we have to provide the system gain $\boldsymbol{K} = \mathbf{10}^{(-\mathbf{23.8/20})} = \mathbf{0.065}$. The complete controller $\boldsymbol{C_{17}}(s)$ can be represented as Eq. (67):

$$\begin{aligned} \boldsymbol{C_{17}}(s) &= \boldsymbol{K} * \boldsymbol{G_{dbz}}(s) \\ &= \frac{\boldsymbol{K} * (s+\mathbf{10})(s+\mathbf{10})}{s} \\ &= \frac{\mathbf{0.065} * (s+\mathbf{10})(s+\mathbf{10})}{s} \\ &= \frac{\mathbf{6.5}\,\mathcal{C}\,\mathbf{1.3}\,\mathcal{C}\,\mathbf{0.065}s^{2}}{s} \\ &= \frac{\boldsymbol{K_i} + \boldsymbol{K_p}s + \boldsymbol{K_d}s^{2}}{s} = \boldsymbol{G_{PID}}(s) \end{aligned} \tag{67}$$

The comparisons of those with or without the system gain $\boldsymbol{K}$ are shown in FIGURE 45. From FIGURE 45, it is clear that when increasing the system gain $\boldsymbol{K}$, the curve of the frequency response follows to translate rightwards and becomes better. Furthermore, the step responses of the "elevator angle to AOA" system are also shown in Table 30.

From FIGURE 45 and Table 30, we can find that our design $\boldsymbol{C_{17}}(s)$ improves both the setting time and overshoot of the system. Especially, this design increases the relative stabilities of the system. It is obvious that gain margin (G.M.) and phase margin (P.M.) all become larger. This improvement helps UAVs to have a greater robustness and survival rate in an uncertain operating environment.

C. CONTROLLER DESIGNS FOR THE CORRECT MODEL OF THE SCALE CESSNA 182 UAV

1) True "elevator angle to angle of attack (AOA)" system

TABLE 30. Step response specifications of the closed-loop system for "elevator angle to AOA" system.

Characteristic	Original System	Original Controller	Our Designed
Controller	—	$\mathbf{C_1(s)}$	$\mathbf{C_{17}(s)}$
Rise time (sec)	0.149	0.07	0.164
Setting time (sec)	27.5	0.7552	0.079
Steady state error	0.353	0	0
Overshoot (OS%)	6.8	7.2808	0
Gain margin (G.M)	14.7	∞	∞
Phase margin (P.M)	109	67.5	70.4

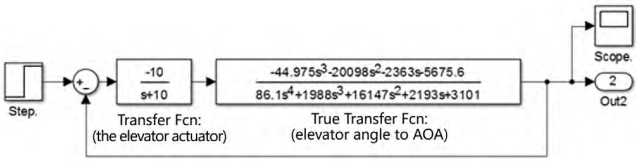

FIGURE 46. Block plot of true "elevator angle to AOA" system.

As we discussed earlier, Yang [12] forgot to change the gravity value 9.8 (N / kg) to $\mathbf{32.174}(ft/sec^{2})$. Therefore, the transfer function of the "elevator angle to AOA" system is not correct. After modifying the gravity value mentioned above, the true transfer function of the "elevator angle to AOA" system is shown in Eq. (68), and the true block diagram is also shown in FIGURE 46:

$$\frac{\alpha_s(s)}{\delta_{E_s}(s)} = \frac{-\mathbf{44.975}s^{3} - \mathbf{20098.4}s^{2} - \mathbf{2363}s - \mathbf{5675.6}}{\mathbf{86.1}s^{4} + \mathbf{1988}s^{3} + \mathbf{16147}s^{2} + \mathbf{2193}s + \mathbf{3101}} \tag{68}$$

By analyzing the pole-zero distribution of the true "elevator angle to AOA" system, we can get the Eq. (69):

$$\begin{cases} \textit{zero} : -446.76, -0.0584 \pm 0.528i \\ \textit{pole} : -10, -0.0568 \pm 0.4379i, \\ \quad -11.4879 \pm 7.2636i \end{cases} \tag{69}$$

By comparing the original and true "elevator angle to AOA" systems from FIGURE 6 and FIGURE 46, it is obvious that these two systems have the similar poles and zeros. Therefore, we can just repeat the same procedures without considering the relative stability in section IVA1 and apply the same method to design a suitable controller. However, this method cannot guarantee how much relative stability our UAV system has. Besides, as we said above in section IVB, in order to enrich the controller designs in this research, we will design the controller with more various modes. In addition, we will also give more instruction to demonstrate how to improve the transient response and steady-state error, and also take relative stability into account at the same time.

About the true "elevator angle to AOA" system, according to FIGURE 46 and Eq. (69), we can find the pole-zero distribution of the open-loop transfer. We designed the mode of the controller $\boldsymbol{C_{18}}(\boldsymbol{s})$ as Eq. (70) and followed the five steps described in section IVB.

$$\boldsymbol{C_{18}}(\boldsymbol{s}) = \frac{\boldsymbol{K_1} * (\boldsymbol{s^2} + \boldsymbol{K_2 s} + \boldsymbol{K_3})}{\boldsymbol{s}} \tag{70}$$

The first step is to select one pole that we wanted to delete in the true "elevator angle to AOA" system. Even here, we choose the value of the unwanted pole to be-10. Besides, for the improvement of the steady-state error, we chose to set the desired pole located at the origin. Therefore, the controller $\boldsymbol{C_{18}}(\boldsymbol{s})$ should contain the term: $\boldsymbol{G_{db}}(\boldsymbol{s}) = \frac{s+10}{s}$. Continuing the steps in section IVB, we will also find the worst phase of the system happened at frequency $\boldsymbol{\omega} = \boldsymbol{140.6}^{\boldsymbol{rad}}/_{\boldsymbol{sec}}$. we assume that the other wanted zero is located at frequency $\boldsymbol{\omega_{cf}}$. Therefore, according to the criterion of the Nichols plot, if we set $\boldsymbol{10\omega_{cf}} \cong \boldsymbol{\omega} = \boldsymbol{140.6}$, we will boost the higher system phase. Hence, the other zero is located at -14.06, and we also get the system gain $\boldsymbol{K} = \boldsymbol{0.0368}$ for the safe UAV G.M. standard. Thence, the complete form of controller $\boldsymbol{C_{18}}(\boldsymbol{s})$ is shown as Eq. (71). The comparisons of the closed-loop responses for the true "elevator angle to AOA" system are shown in FIGURE 47 and in Table 31. Additionally, FIGURE 48 also illustrates the stability improvement of our designed controller.

$$\boldsymbol{C_{18}}(\boldsymbol{s}) = \frac{\boldsymbol{0.0368}(\boldsymbol{s^2} + \boldsymbol{24.06 s} + \boldsymbol{140.6})}{\boldsymbol{s}} \tag{71}$$

In Table 31, we can see that after cascading our controller $\boldsymbol{C_{18}}(\boldsymbol{s})$, the true "elevator angle to AOA" system has $\boldsymbol{G.M} = \boldsymbol{\infty dB}$ and $\boldsymbol{P.M} = \boldsymbol{69.5}°$. Therefore, the controller $\boldsymbol{C_{18}}(\boldsymbol{s})$ helps to improve the system to be better than the design standard of US military [16]. Also, from Table 31, FIGURE 47 and FIGURE 48 it is also obvious that our design $\boldsymbol{C_{18}}(\boldsymbol{s})$ not only improves the transient response and steady-state error but also enhances the relative stability at the same time.

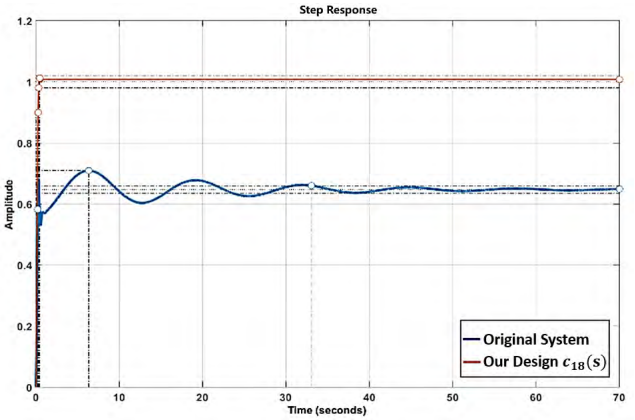

FIGURE 47. Step response of the closed-loop system for the true "elevator angle to AOA" system (Original System) and the system cascaded Our Design $C_{18}(s)$.

TABLE 31. Comparisons of the closed-loop responses for the true "elevator angle to AOA" system.

Characteristic	Original System	Our Design
Controller	–	$\mathbf{C_{18}(s)}$
Setting time (sec)	33.1	0.33
Steady state error	0.35	0
Overshoot (OS%)	9.64	1.11
Gain margin (G.M)	14.8	∞
Phase margin (P.M)	109	69.5

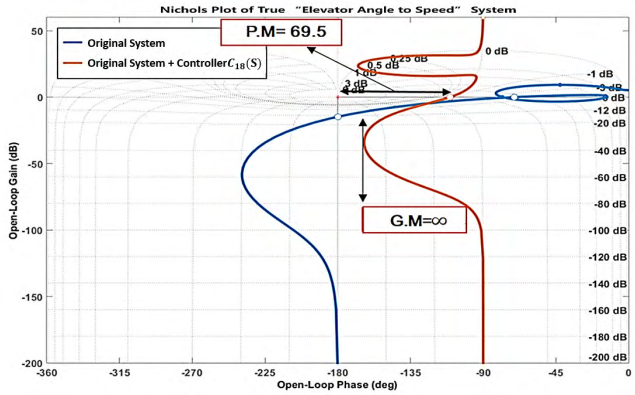

FIGURE 48. Nichols plot of the true "elevator angle to AOA" system with Our Design $C_{18}(s)$.

2) True "elevator angle to speed" system

The transfer function of the true "elevator angle to speed" system is shown as Eq. (72), and the block diagram after correction is shown in FIGURE 49.

$$\frac{\boldsymbol{u_s}(\boldsymbol{s})}{\boldsymbol{\delta_{E_s}}(\boldsymbol{s})} = \frac{-\boldsymbol{875.2 s^2} + \boldsymbol{248865 s} + \boldsymbol{3318832}}{\boldsymbol{86.1 s^4} + \boldsymbol{1988 s^3} + \boldsymbol{16147 s^2} + \boldsymbol{2193 s} + \boldsymbol{3101}} \tag{72}$$

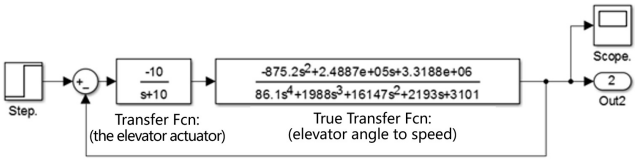

FIGURE 49. Block diagram of true "elevator angle to speed" system.

Upon analyzing the pole-zero distribution of the true "elevator angle to speed" system, we can get the Eq. (73):

$$\begin{cases} \textit{zero} : -12.763,\ 297.1152 \\ \textit{pole} : -10,\ -0.0568 \pm 0.4379i, \\ \quad -11.4879 \pm 7.2636i \end{cases} \tag{73}$$

From Eq. (73), we found out that the pole-zero distribution of the true "elevator angle to speed" system resembles one of the original "elevator angle to speed" system in [12]. It also has a zero located at RHS of the s-plane. This system is a non-minimum phase system, and the step response of this closed-loop system is divergent, too. Therefore, we can follow the procedures in section IVA2 to design our innovative controller: "Reverse Gain PID Controller".

The controller $\boldsymbol{C_{19}(s)}$ for the true "elevator angle to speed" system is shown as Eq. (74). Then, we repeated the first three steps in section IVA2, and get the parameters: $\boldsymbol{K_1 = -0.0041}$, $\boldsymbol{K_2 = 0.37}$, and $\boldsymbol{K_3 = 0.14}$. The Eq. (74) can be arranged to Eq. (75):

$$\boldsymbol{C_{19}(s) = \frac{-K_1 * (s^2 + K_2 s + K_3)}{s}} \tag{74}$$

$$\boldsymbol{C_{19}(s) = \frac{-0.0041(s^2 + 0.37s + 0.14)}{s}} \tag{75}$$

Upon cascading Eq. (75) before the true "elevator angle to speed" system in FIGURE 49, and applying the Matlab/Simulink, we can get the results of the step response and relative stability as shown in FIGURE 50, FIGURE 51, and Table 32. From FIGURE 20, FIGURE 51, and Table 32, we found that our controller, $\boldsymbol{C_{19}(s)}$, does help overcome the negative effect from the non-minimum phase system, and it really stabilizes the divergent system. Likewise, this design also guarantees the true "elevator angle to speed" system with the relieved relative stability ($\boldsymbol{G.M = 27.1dB > 6dB}$, $\boldsymbol{P.M = 66.1^\circ > 60^\circ}$).

3) True "elevator angle to pitch angle" system

The transfer function of the true "elevator angle to pitch angle" system is shown as Eq. (76), and the block diagram after correction is shown in FIGURE 52.

$$\frac{\boldsymbol{\theta_s(s)}}{\boldsymbol{\delta_{E_s}(s)}} = \frac{\boldsymbol{-19887s^2 - 105491s - 15562}}{\boldsymbol{86.1s^4 + 1988s^3 + 16147s^2 + 2193s + 3101}} \tag{76}$$

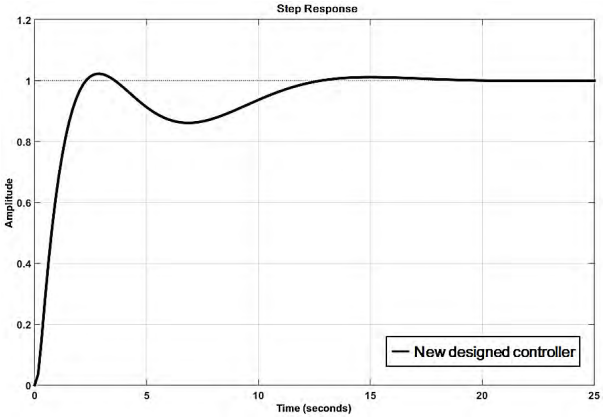

FIGURE 50. Closed-loop response of the true "elevator angle to speed" system with controller $C_{19}(s)$.

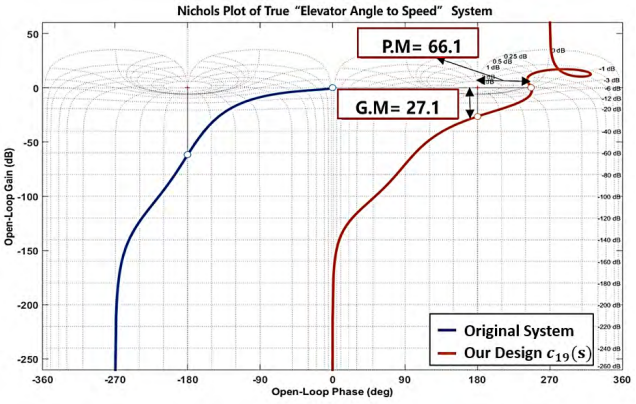

FIGURE 51. Nichols plot of the true "elevator angle to speed" system with controller $C_{19}(s)$.

TABLE 32. Comparisons of the closed-loop responses for the true "elevator angle to speed" system.

Characteristic	Original System	Our Design
Controller	—	$\mathbf{C_{19}(s)}$
Rise time (sec)	System is divergent	1.43
Setting time (sec)	System is divergent	11.6
Steady state error	System is divergent	0
Overshoot (OS%)	System is divergent	2.19
Gain margin (G.M)	System is divergent	2.71
Phase margin (P.M)	System is divergent	66.1

After analyzing the pole-zero distribution of the true "elevator angle to pitch angle" system, we can get the Eq. (77):

$$\begin{cases} \textit{zero} : -0.152,\ -5.1489 \\ \textit{\&pole} : -10,\ -0.0568 \pm 0.4379i, \\ \quad -11.4879 \pm 7.2636i \end{cases} \tag{77}$$

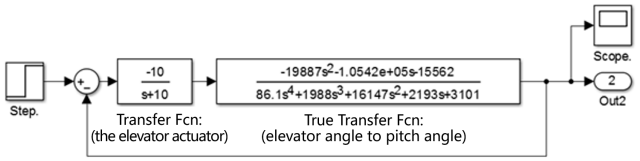

FIGURE 52. Block diagram of true "elevator angle to pitch angle" system.

Upon comparing the pole-zero distributions from Eq. (77) and Eq. (49), we can find that the "component" of the true "elevator angle to pitch angle" system is better than one of the original "elevator angle to pitch angle" in section IVA1, since the true "elevator angle to pitch angle" system is a minimum phase system, and the original "elevator angle to pitch angle" system has an unstable zero: 0.1519.

Of course, we can just repeat the steps of designing the "Reverse Gain PID Controller" mentioned above. However, since we wanted to strengthen the relative stability of the UAV system, for safety reasons, we followed the steps of the robust controller in section IVB and tried to handle the non-minimum phase system. In the first step, we chose the unwanted pole, -10, of the original "elevator angle to pitch angle" system. Therefore, our designed controller should contain a term $\boldsymbol{G_{db}}(\boldsymbol{s}) = \frac{\boldsymbol{s+10}}{\boldsymbol{s}}$ (shown in Eq. (78)):

$$\boldsymbol{G_{db}}(\boldsymbol{s}) = \frac{\boldsymbol{s+10}}{\boldsymbol{s}} \tag{78}$$

Secondly and thirdly, when cascading the $\boldsymbol{G_{db}}(\boldsymbol{s})$ before Eq. (76) and drawing the Nichols plot or Bode plot, we can get the frequency response of the true "elevator angle to pitch angle" system (shown in FIGURE 53). In FIGURE 53, after adding a zero, -10, we can find that the whole system phase is pulled up to above $-\boldsymbol{180^o}$. Thus, the G.M. became $\infty\boldsymbol{dB}$. However, we must be careful with the other zero selection. It must be located on positive or flat slopes of the phase curve or the phase of the other zero will be offset. Therefore, based on this consideration, we chose $\boldsymbol{\omega = 1}$ to be the location of the other zero.

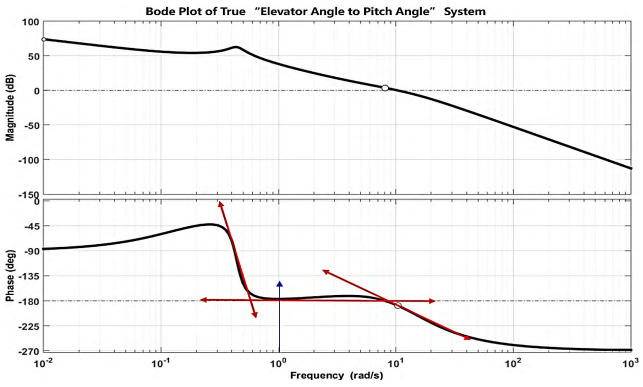

FIGURE 53. Bode plot of the true "elevator angle to pitch angle" system with the $G_{db}(s)$.

The fourth step is to combine the selected zero in the previous step with $\boldsymbol{G_{db}}(\boldsymbol{s})$. Then, the result $\boldsymbol{G_{dbz}}(\boldsymbol{s})$ and the

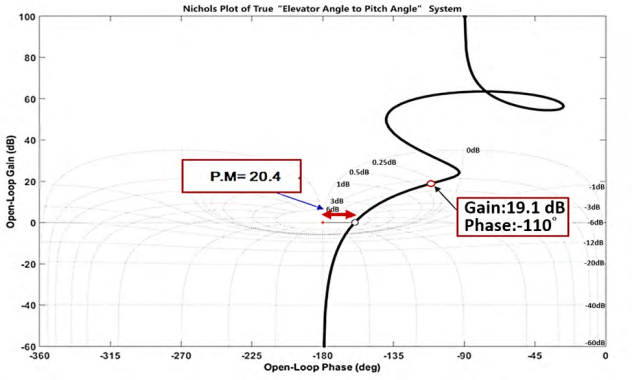

FIGURE 54. Nichols plot of the true "elevator angle to pitch angle" system with the $G_{dbz}(s)$.

controller $\boldsymbol{C_{20}}(\boldsymbol{s})$ can be represented as Eq. (79) and Eq. (80). After we choose the finally optimal phase position, we can come back to get the desired system $\boldsymbol{K}$ value.

$$\boldsymbol{G_{dbz}}(\boldsymbol{s}) = \frac{(\boldsymbol{s+10})(\boldsymbol{s+1})}{\boldsymbol{s}} \tag{79}$$

$$\boldsymbol{C_{20}}(\boldsymbol{s}) = \frac{\boldsymbol{K} * (\boldsymbol{s+10})(\boldsymbol{s+1})}{\boldsymbol{s}} \tag{80}$$

After cascading $\boldsymbol{G_{dbz}}(\boldsymbol{s})$ with the true "elevator angle to pitch angle", the system G.M. becomes ∞ and P.M. becomes $\boldsymbol{33.8^o}$ (shown in FIGURE 54).

If we want to pull $\boldsymbol{P.M}$ up to $\boldsymbol{70^\circ}$, we must make the gain $\boldsymbol{0dB}$ at location phase $\boldsymbol{-110^o}$. Repeating the fifth step of the robust controller in section IVB, this desired position is located at $(\boldsymbol{-110^o}, \boldsymbol{19.1dB})$ now. If we want the curve to pass the 0dB location, we must supply the system gain value: $\boldsymbol{K = 10^{-19.1/20} = 0.11}$. Therefore, controller $\boldsymbol{C_{20}}(\boldsymbol{s})$ can be rearranged as Eq. (81).

$$\boldsymbol{G_{20}}(\boldsymbol{s}) = \frac{\boldsymbol{0.11} * (\boldsymbol{s+10})(\boldsymbol{s+1})}{\boldsymbol{s}} \tag{81}$$

Now, we cascade $\boldsymbol{C_{20}}(\boldsymbol{s})$ in Eq. (81) before the true "elevator angle to pitch angle" and draw the Nichols plot (shown in FIGURE 55). When comparing FIGURE 54 and FIGURE 55, we find that the advantage of the system gains $\boldsymbol{K}$. Apart from this, the comparisons of those with or without the controller $\boldsymbol{C_{20}}(\boldsymbol{s})$ are also shown as FIGURE 56 and Table 32. It is very obvious that after cascading our designed controller $\boldsymbol{C_{20}}(\boldsymbol{s})$, $\boldsymbol{G.M} = \infty\boldsymbol{dB} > \boldsymbol{6dB}$, $\boldsymbol{P.M} = \boldsymbol{69.5^\circ} > \boldsymbol{60^\circ}$. The system performances are improved and already meet the U.S. military standards [16].

4) True "rudder angle to sideslip angle" system

The transfer function of the true "rudder angle to sideslip angle" system is shown as Eq. (82), as shown at the bottom the next page, and the block diagram after correction is shown in FIGURE 57.

We divided the common factor "s" of the open-loop transfer. After analyzing the pole-zero distribution of the true

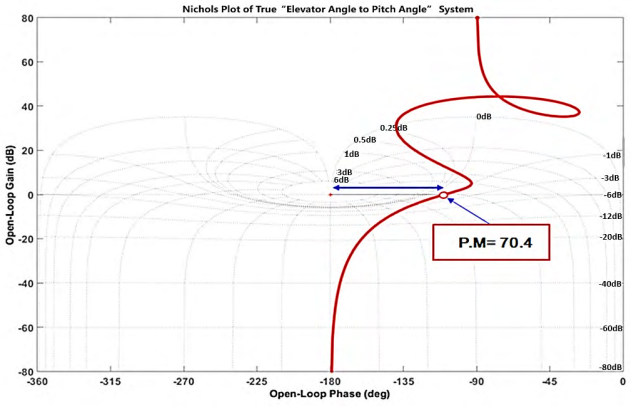

FIGURE 55. Nichols plot of the true "elevator angle to pitch angle" system with the $C_{20}(s)$.

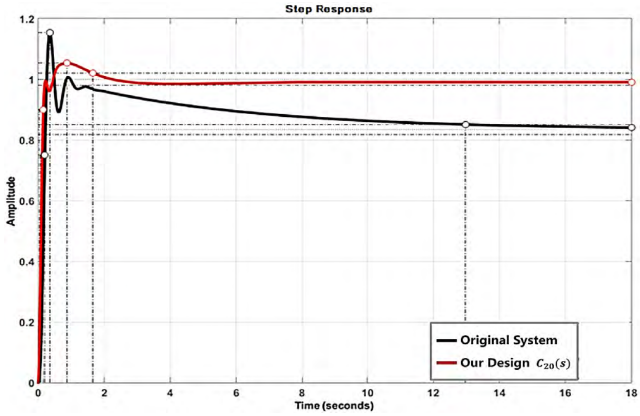

FIGURE 56. Comparisons of the closed-loop responses for the true "elevator angle to pitch angle" system.

TABLE 33. Closed-loop responses based on the transfer function of true "elevator angle to pitch angle" system.

Characteristic	Original System	Our Design
Controller	–	$\mathbf{C_{20}(s)}$
Rise time (sec)	0.133	0.123
Setting time (sec)	13	1.65
Steady state error	0.834	0
Overshoot (OS%)	38.8	5.45
Gain margin (G.M)	10	∞
Phase margin (P.M)	52.7	70.2

"rudder angle to sideslip angle" system, we can get Eq. (83):

$$\begin{cases} \boldsymbol{zero}: \mathbf{0.0445}, \mathbf{-34.2776}, \mathbf{-297.1067} \\ \boldsymbol{pole}: \mathbf{-0.0461}, \mathbf{-10}, \mathbf{-33.5475}, \\ \quad \mathbf{-1.7274 \pm 8.1877}\boldsymbol{i} \end{cases} \tag{83}$$

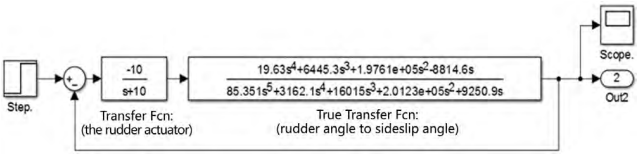

FIGURE 57. Block diagram of true "rudder angle to sideslip angle" system.

TABLE 34. The comparison of reference and Initial design.

Characteristic	Original System	Our Design
Controller	–	$\mathbf{C_{21}(s)}$
Rise time (sec)	System is divergent	0.24
Setting time (sec)	System is divergent	1.49
Steady state error	System is divergent	0
Overshoot (OS%)	System is divergent	4.005
Gain margin (G.M)	System is divergent	∞
Phase margin (P.M)	System is divergent	66.3

From Eq. (83), we discovered that the pole-zero distribution of the true "rudder angle to sideslip angle" system has a zero located at the RHS of the s-plane, and it is similar to the original "rudder angle to sideslip angle" system in section IVA2. Therefore, we can repeat the same method to design our innovative controller: "Reverse Gain PID Controller".

In this section, the controller $\boldsymbol{C_{21}(s)}$ for the true "rudder angle to sideslip angle" system is shown as Eq. (84). We repeated the first three steps in section IVA2, and get the parameters: $\boldsymbol{K_1} = \mathbf{-0.095284}$, $\boldsymbol{K_2} = 3.87$, and $\boldsymbol{K_3} = \mathbf{68.1}$. Hence, the Eq. (84) can be arranged to Eq. (85):

$$\boldsymbol{C_{21}(s)} = \frac{-\boldsymbol{K_1} * (\boldsymbol{s^2} + \boldsymbol{K_2 s} + \boldsymbol{K_3})}{\boldsymbol{s}} \tag{84}$$

$$\boldsymbol{C_{21}(s)} = \frac{\mathbf{-0.095284}(\boldsymbol{s^2} + \mathbf{3.87}\boldsymbol{s} + \mathbf{68.1})}{\boldsymbol{s}} \tag{85}$$

After cascading Eq. (85) before the true "rudder angle to sideslip angle" system in FIGURE 57, and applying the Matlab/Simulink, we can get the results of the step response and relative stability as shown in FIGURE 58, FIGURE 59, and Table 34. From the FIGURE 58, FIGURE 59, and 33, we find out that our controller, $\boldsymbol{C_{21}(s)}$, really helps to overcome the negative effect from non-minimum phase system, and it does stabilize the divergent system. Moreover, our controller also ensures the true "rudder angle to sideslip angle" system with enough relieved relative stability ($\boldsymbol{G.M} = \infty \boldsymbol{dB} > \mathbf{6}\boldsymbol{dB}$, $\boldsymbol{P.M} = \mathbf{66.3}^\circ > \mathbf{60}^\circ$).

5) True "aileron angle to roll angle" system

$$\frac{\boldsymbol{\beta_s(s)}}{\boldsymbol{\delta_{R_s}(s)}} = \frac{\mathbf{19.63}\boldsymbol{s^3} + \mathbf{6445.31}\boldsymbol{s^2} + \mathbf{197608.2}\boldsymbol{s} - \mathbf{8814.6}}{\mathbf{85.3511}\boldsymbol{s^4} + \mathbf{3162.13}\boldsymbol{s^3} + \mathbf{16014.5182}\boldsymbol{s^2} + \mathbf{201227.02}\boldsymbol{s} + \mathbf{9250.934}} \tag{82}$$

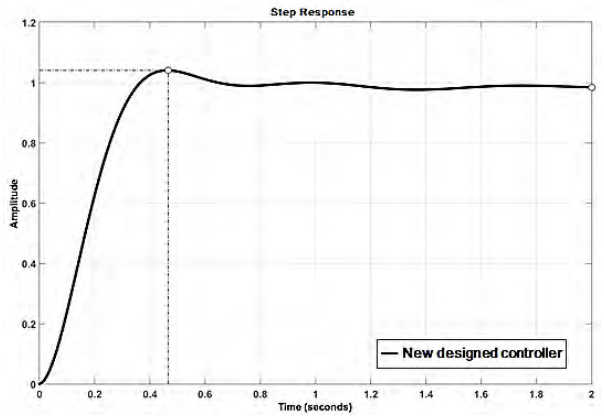

FIGURE 58. Closed-loop response of the true "rudder angle to sideslip angle" system with controller $C_{21}(s)$.

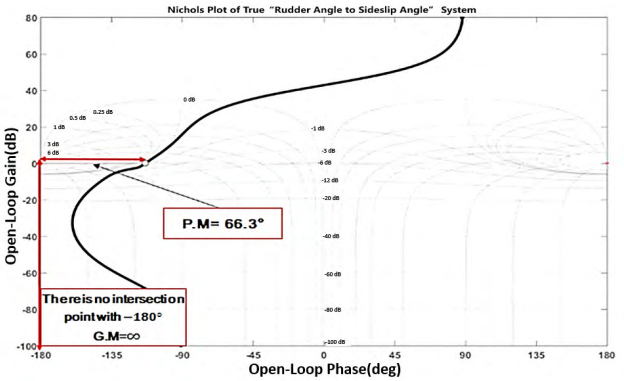

FIGURE 59. Nichols plot of the true "rudder angle to sideslip angle" system with controller $C_{21}(s)$.

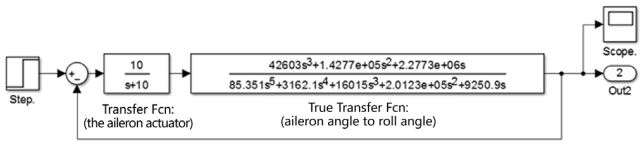

FIGURE 60. Block diagram of true "aileron angle to roll angle" system.

The transfer function of the true "aileron angle to roll angle" system is shown as Eq. (86), as shown at the bottom of this page, and the block diagram after correction is shown in FIGURE 60.

We divided the common factor "s" of the open-loop transfer. After analyzing the pole-zero distribution of the true "aileron angle to roll angle" system, we can get Eq. (87):

$$\begin{cases} \boldsymbol{zero}: -1.6756 \pm 7.1166\boldsymbol{i} \\ \boldsymbol{pole}: -0.0461, -10, -33.5475, \\ \quad -1.7274 \pm 8.1877\boldsymbol{i} \end{cases} \tag{87}$$

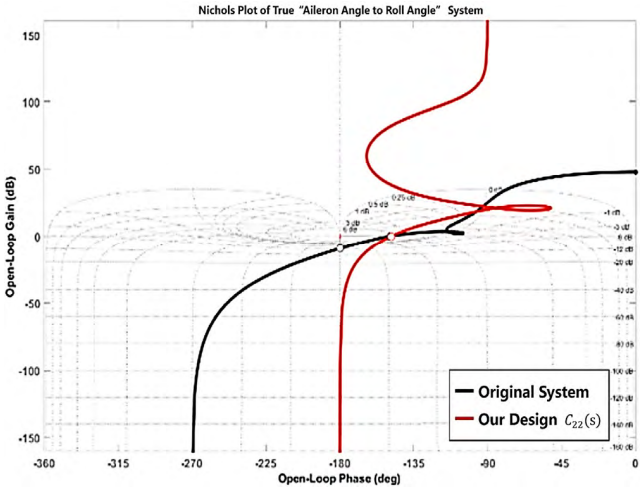

FIGURE 61. Nichols plot of the true "aileron angle to roll angle" system with initial design $C_{22}(s)$.

From Eq. (87), we can find that there has a pole near the origin, and we have to be careful about the stability problem. We set the desired controller $\boldsymbol{C_{22}}(\boldsymbol{s})$ to be in the form as shown in Eq. (88), and followed the design procedures in section IVA1 to deal with the normal minimum phase system, then naturally, we can get $\boldsymbol{K_1} = 4.8$, and $\boldsymbol{K_2} = 8.6$. The desired controller is represented as Eq. (89):

$$\boldsymbol{C_{22}}(\boldsymbol{s}) = \frac{\boldsymbol{s^2} + \boldsymbol{K_1 s} + \boldsymbol{K_2}}{\boldsymbol{s}} \tag{88}$$

$$\boldsymbol{C_{22}}(\boldsymbol{s}) = \frac{\boldsymbol{s^2} + 4.8\boldsymbol{s} + 8.6}{\boldsymbol{s}} \tag{89}$$

By cascading Eq. (88) before the true "aileron angle to roll angle" system in FIGURE 60, and applying the Matlab/Simulink, we can get the Nichols plot as shown in FIGURE 61. From FIGURE 61, we can get the relative stability: $\boldsymbol{G.M} = \infty \boldsymbol{dB}, \boldsymbol{P.M.} = 30.6°$. We applied the fifth step of the controller design in section IV2 to find the suitable system gain $\boldsymbol{K}$. We discovered that if we provide the system gain $\boldsymbol{K} = 0.184$, we will pull the $\boldsymbol{P.M.}$ up close to $70°$ (shown in FIGURE 61). Therefore, our initial design $\boldsymbol{C_{22}}(\boldsymbol{s})$ should be adjusted to the new controller $\boldsymbol{C_{23}}(\boldsymbol{s})$ (shown in Eq. (90)):

$$\boldsymbol{C_{23}}(\boldsymbol{s}) = \frac{0.184 * (\boldsymbol{s^2} + 4.8\boldsymbol{s} + 8.6)}{\boldsymbol{s}} \tag{90}$$

Cascading Eq. (90) before the true "aileron angle to roll angle" system in FIGURE 60, and applying the Matlab/Simulink again, we can get the new Nichols plot as shown in FIGURE 62, closed-loop response as shown in FIGURE 63 and in Table 35. From FIGURE 62 and Table 35, it is very clear that our controller does improve

$$\frac{\boldsymbol{\phi_s}(\boldsymbol{s})}{\boldsymbol{\delta_{A_s}}(\boldsymbol{s})} = \frac{42602.9\boldsymbol{s^2} + 142774.845\boldsymbol{s} + 2277257}{85.3511\boldsymbol{s^4} + 3162.13\boldsymbol{s^3} + 16014.5182\boldsymbol{s^2} + 201227.02\boldsymbol{s} + 9250.934} \tag{86}$$

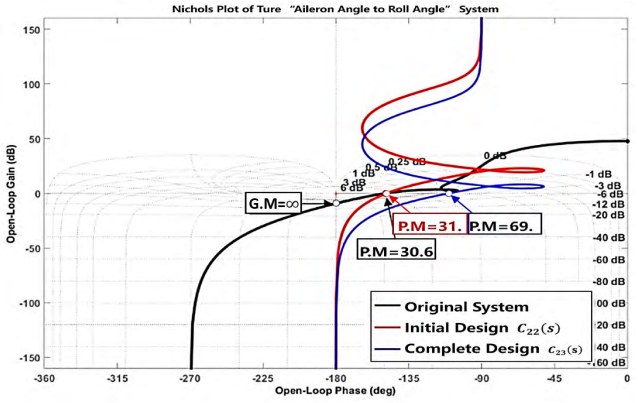

FIGURE 62. Nichols plot of the true "aileron angle to roll angle" system with controller $C_{23}(s)$.

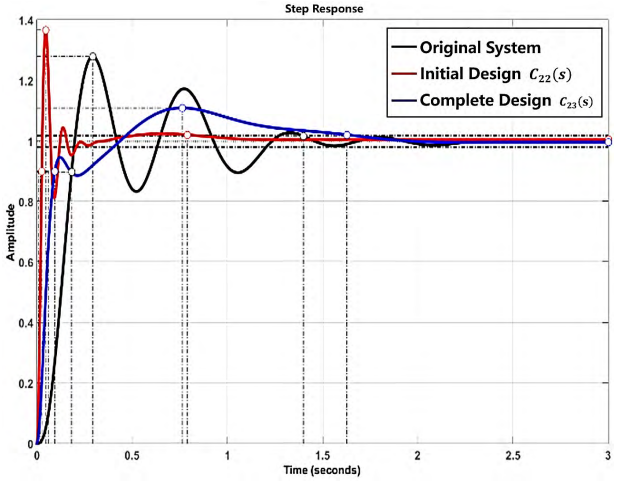

FIGURE 63. Closed-loop response of the true "aileron angle to roll angle" system (Original system) and with different controllers.

the relative system and meet the UAV safety requirement ($G.M = \infty dB > 6dB$, $P.M = 69.5° > 60°$). However, from FIGURE 63 and Table 35, we found that it is a little bit worse in the parts of the rising time and setting time since we chose to improve the overshoot and relative stability of the system. Because of the fact that we thought the safety and survival are the most important requirements for the UAV systems, we exchanged a little bit of the rising time and setting time for the smaller overshoot and relative stability. Of course, the designer can also adjust the different system gain K to have different system performance according to their demands.

6) True "rudder angle to yaw angle" system

The transfer function of the true "rudder angle to yaw angle" system is shown as Eq. (91), as shown at the bottom of this page, and the block diagram after correction is shown in FIGURE 64:

TABLE 35. Closed-loop response of the true "aileron angle to roll angle" system (Original system) and with different controllers.

Characteristic	Original System	Initial Designed	Complete Designed
Controller	—	$C_{22}(s)$	$C_{23}(s)$
Rise time (sec)	0.121	0.0188	0.0768
Setting time (sec)	1.4	0.79	1.63
Steady state error	0	0	0
Overshoot (OS%)	28.4	36.6	10.9
Gain margin (G.M)	9.3	∞	∞
Phase margin (P.M)	30.6	31.3	69.8

After analyzing the pole-zero distribution of the true "rudder angle to yaw angle" system, we can get Eq. (92):

$$\begin{cases} zero : -33.9737, -0.0922 \pm 1.3785i \\ pole : 0, -0.0461, -10, -33.5475, \\ \quad -1.7274 \pm 8.1877i \end{cases} \tag{92}$$

From Eq. (92), we can find that there is a pole near the origin and also a pair complex-conjugate poles close to the jw-axis. Moreover, we should be careful with stability problem. Furthermore, this system is a system type one. Hence, we should not design the PI and PID controllers, but we can design the "complex-conjugate zeros controller" which we created in section IVA6. We set this controller form as the Eq. (93), where K_1 and K_2 are constants, and K is the system gain.

$$C_{24}(s) = K * (s^2 + K_1 s + K_2) \tag{93}$$

We applied the RC criterion in section IVA1 to get the values of K_1 and K_2, then we get $K_1 = 26.1$ and $K_2 = 340$. We applied the Matlab (command: rlocus), then we can get the system gain $K = 2$. Therefore, the "complex-conjugate zeros controller" for the true "rudder angle to yaw angle"

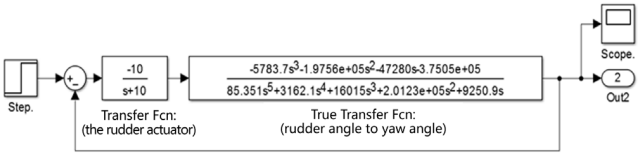

FIGURE 64. Block diagram of the true "rudder angle to yaw angle" system.

$$\frac{\psi_s(s)}{\delta_{R_s}(s)} = \frac{-5783.689s^3 - 197559.897s^2 - 47279.626s - 375046.03}{85.3511s^5 + 3162.13s^4 + 16014.5182s^3 + 201227.02s^2 + 9250.934s} \tag{91}$$

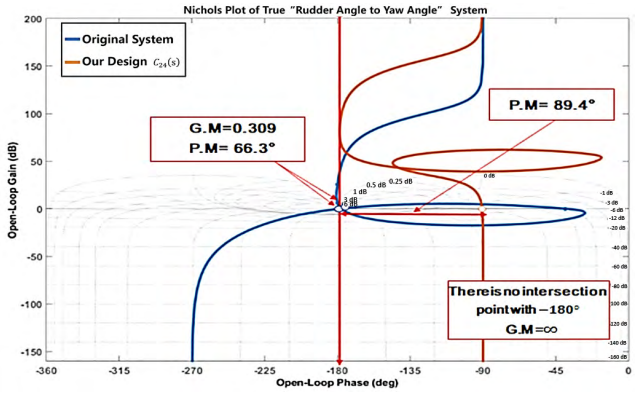

FIGURE 65. Nichols plot of the true "rudder angle to yaw angle" system with controller $C_{24}(s)$.

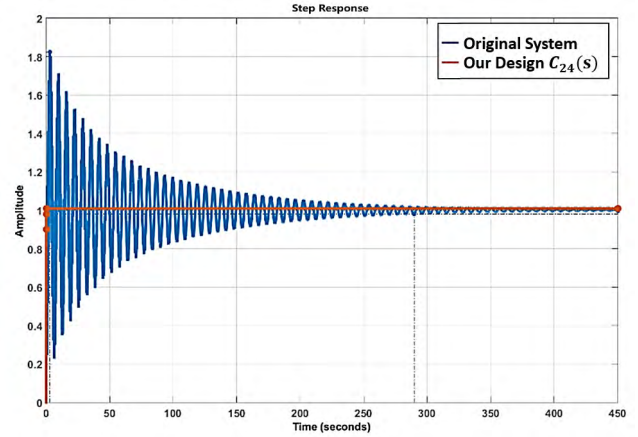

FIGURE 66. Comparisons of the closed-loop responses for the true "rudder angle to yaw angle" system.

system can be represented as Eq. (94):

$$C_{24}(s) = 2*(s^2 + 26.1s + 340) \tag{94}$$

Upon cascading Eq. (94) before the true "rudder angle to yaw angle" system in FIGURE 64, and applying the Matlab/Simulink, we can get the Nichols plot as FIGURE 65, closed-loop response as FIGURE 66 and Table 36. From FIGURE 65 and Table 35, it is very obvious that our controller $C_{24}(s)$ really improves the relative system and meets the UAV safety requirement ($G.M = \infty dB > 6dB$, $P.M = 89.4° > 60°$). Besides, we can also observe that our new mode controller, $C_{24}(s)$, can improve both the transient response and the steady-state error, simultaneously.

V. CONCLUSION

The main objective of this research is to analyze the UAV system, scale Cessna 182, and design suitable controllers according to the system properties and the task requirements. Different from Ziegler–Nichols method and other common trial and error methods, the controller designs in this paper apply the model reduction method, RL, RC, pole-zero placement, frequency response, and orthodox PID criterion that

TABLE 36. Step response specifications of the closed-loop system for TRUE "rudder angle to yaw angle" system.

Characteristic	Original System	Complete Designed
Controller	—	$C_{24}(s)$
Rise time (sec)	1.63	0.00158
Setting time (sec)	10.1	0.00263
Steady state error	10.2	0
Overshoot (OS%)	33.1	0.845
Gain margin (G.M)	0.309	∞
Phase margin (P.M)	1.63	89.4

help operators to design more suitable controllers. In addition, the designed controller based on RC is more flexible when facing sudden difficulties or demands (emergencies/abrupt situations).

Additionally, RC reflects the relationship and influences among the controller parameters, and helps in designing a reasonable and reliable controller to improve the response performance and accuracy of the system.

Furthermore, due to the non-minimum phase system of the scale Cessna 182 system, Ziegler–Nichols method can't solve the problem. In this paper, we created a new design method called "Reverse Gain PID Controller" to help overcome the negative effects from non-minimum phase, and stabilize the divergent system. In addition, not only our designed controller improves both the transient response and steady-state error but also enhances the relative stability of the system, simultaneously. In summary, as what we described in the introduction, the research done in this paper has the following five contributions.

1) According to the characteristics of 12 different UAV systems, a variety of controllers have been designed. Therefore, the adopted design would be from paper which has the most extensive analysis for the controller designs of UAV motions. The content of the paper is rich and highly applicable and can be used as a source of study by relevant researchers.
2) The controllers of this research not only improve the system responses of UAVs in time domain, but also emphasize the response analysis in frequency domain and the designs of the robust controller. Therefore, the designed controllers can give the systems better relative stabilities that can increase the UAVs' robustness and survival rate when operating in unknown environments.
3) In the face of the unstable non-minimum phase system, this study proposes "Reverse Gain PID Controller" to deal with it. In addition to effectively improve the system response, "Reverse Gain PID Controller" also

ameliorates the relative stability of the system at the same time.

4) The "Reverse Gain PID Controller" is easier to implement than other methods that can improve non-minimum phase systems, and it is not as complicated in operation as other methods. Besides, it has a better improvement in terms of the coupling effect between the inverse response and the settling time of the non-minimum phase systems.
5) The root contour theory was applied in the controller design process, which has a higher degree of accuracy and effectiveness in the selection of the multi-parameters of the controllers.

We summarize the contribution of this research basing on the content as the following 4 superiority:

1) Most UAV researches only discuss the longitudinal movement of flight. However, the scope of this study includes the longitudinal motion and lateral motion. A variety of controllers have been designed for 12 different UAV subsystems, so this study is probably the most comprehensive research on UAV flight motion.
2) The parameters of the PID controller in this thesis are obtained by combining the Root Locus and Root Contour theory. The method is theoretical, applicable and flexible in design, and the system response is better. It is not like the Ziegler-Nichols method in the general literature. The roughness controller parameters based on Ziegler-Nichols method are inaccurate and inelastic.
3) In addition, to illustrating the relationship between system response and single parameter adjustment, Root Contour, as applied in this study, can show the interaction between multiple parameters in the controller when they are adjusted. The coupling effect between these parameters adjustment will seriously affect the follow-up system response, so it is extremely important. However, there is no literature to discuss this argument now.
4) The "Reverse Gain PID Controller" we created in this study not only improved the transient response and steady-state error of the non-minimum-phase systems, but also increased the relative stability of the system at the same time. In addition, "Reverse Gain PID Controller" has a better result on the coupling effect between the reverse response and the setting time of the non-minimum phase system. And most importantly, this method is extremely versatile and very efficient. Thus, users won't face difficulties controlling in regards to their background and connotation.

As for the limitation part of the controller design in this study, according to our simulation results, in the case that system parameters of UAV are known, the methods of the controller designs in this research are always feasible without applying restrictions. As for the hardware limitations, the result will be shown after the field tests of UAV hardware.

Finally, this research content is academic, practical, and very efficient in nature, and can also be referred to and applied by researchers who wish to carry out further follow-up research.

REFERENCES

[1] X. Zhao, P. Shi, X. Zheng, and J. Zhang, "Intelligent tracking control for a class of uncertain high-order nonlinear systems," *IEEE Trans. Neural Netw. Learn. Syst.*, vol. 27, no. 9, pp. 1976–1982, Aug. 2015.
[2] X. Zhao, H. Yang, W. Xia, and A. Wang, "Adaptive fuzzy hierarchical sliding-mode control for a class of MIMO nonlinear time-delay systems with input saturation," *IEEE Trans. Fuzzy Syst.*, vol. 25, no. 5, pp. 1062–1077, Jul. 2016.
[3] H. Wang, P. X. Liu, and A. Shi, "Observer-based fuzzy adaptive output-feedback control of stochastic nonlinear multiple time-delay systems," *IEEE Trans. Cybern.*, vol. 47, no. 9, pp. 2568–2578, Feb. 2017.
[4] H. Wang and P. X. Liu, "Robust fuzzy adaptive tracking control for nonaffine stochastic nonlinear switching systems," *IEEE Trans. Cybern.*, vol. 48, no. 8, pp. 2462–2471, Dec. 2017.
[5] X. Hu, L. Wu, X. Si, and B. Xu, "Adaptive sliding mode control of nonlinear non-minimum phase system with input delay," *IET Control Theory Appl.*, vol. 11, no. 8, pp. 1153–1161, May 2017.
[6] M. I. Ahmed and A. Azad, "Mathematical modeling and DLQR based controller design for a non-minimum phase electro hydraulic servo system (EHS)," in *Proc. IEEE Region Conf. (TENCON)*, Feb. 2017, pp. 1839–1844.
[7] Y. Zhang, Q. Zhu, and R. Xiong, "Pre-action and stable inversion based precise tracking for non-minimum phase system," in *Proc. IEEE 55th Conf. Decis. Control (CDC)*, Dec. 2016, pp. 5682–5687.
[8] X. Wang and D. Chen, "Causal inversion of nonminimum phase systems," in *Proc. 40th IEEE Conf. Decis. Control*, Dec. 2001, pp. 73–78.
[9] (Jul. 26, 2017). *The Scale Cessna 182*. [Online]. Available: http://img1.windmsn.com/b/3/323/32398/3239873.jpg
[10] (Jul. 26, 2017). *The Structure of Scale Cessna 182*. [Online]. Available: https://img.ruten.com.tw/s2/0/d8/0e/11090715184142760.jpg
[11] (Jul. 26, 2017). *The Structure of Scale Cessna 182*. [Online]. Available: http://img.banggood.com/images/upload/2015/03/SKU156102-2.jpg
[12] C.-Y. Yang, "On the modeling and stability augmentation of a scale unmanned aerial vehicle," M.S. thesis, Dept. Aerosp. Syst. Eng., Feng Chia Univ., Taichung, Taiwan, 2013.
[13] (Jul. 26, 2017). *The Skylane CESSNA 182 1.6 m Wingspan (747-3)*. [Online]. Available: http://www.exhobby.com/product/74703
[14] M. R. Napolitano, *Aircraft Dynamics: From Modeling to Simulation*. Hoboken, NJ, USA: Wiley, 2012.
[15] (Jul. 26, 2017). *The PID Controller*. [Online]. Available: https://zh.wikipedia.org/wiki/PID%E6%8E%A7%E5%88%B6%E5%99%A8
[16] *Flight Control Systems-Design, Installation and Test of Piloted Aircraft*, document MIL-DTL-9490E, Apr. 2008.
[17] S. Bogos and I. Store, "Similarity criteria for 'full' and 'scale' aircraft on the lateral stabilty analysis," *U.P.B. Sci. Bull., Serial D*, vol. 74, no. 4, pp. 14–26, 2012.
[18] W. W. Durgin and C.-W. Kim, "Scale modeling of Cessna 172," Amer. Inst. Aeronaut. Astronaut., San Diego, CA, USA, 2011, pp. 1–9.
[19] J. Chambers, *Modeling Flight: The Role of Dynamically Scaled Free-Flight Models in Support of NASA's Aerospace Programs*. Washington, DC, USA: National Aeronautics and Space Administration, 2010.
[20] M. Shino and M. Nagai, "Yaw-moment control of electric vehicle for improving handling and stability," *JSAE Rev.*, vol. 22, no. 4, pp. 473–480, 2001.
[21] M. Abe, Y. Kano, K. Suzuki, Y. Shibahata, and Y. Furukawa, "Side-slip control to stabilize vehicle lateral motion by direct yaw moment," *JSAE Rev.*, vol. 22, no. 4, pp. 413–419, 2001.
[22] N. S. Nise, *Control Systems Engineering, International Student Version*, 6th ed. Hoboken, NJ, USA: Wiley, 2011.

JIA-HORNG YANG received the M.S. degree in electrical and electronic engineering from the Chung Cheng Institute of Technology (CCIT), National Defense University (NDU), Taoyuan, Taiwan, in 2000, and the Ph.D. degree in electrical and computer engineering from the Naval Postgraduate School (NPS), CA, USA, in 2009. After graduating from NPS, he was a Research and Development Officer with the Weapon System Center, CCIT, NDU. Since 2010, he has been an Assistant Professor with the Electrical and Electronic Engineering Department, CCIT, NDU. From 2011 to 2012, he was also a Leader of Electro-Optical Graduate School, CCIT.

His research interest includes the automatic control system, adaptive control system, digital signal processing, and estimation and tracking.

HUA-KAI XU received the B.S. degree in electrical and electronic engineering and the M.S. degree from the Chung Cheng Institute of Technology (CCIT), National Defense University, Taoyuan, Taiwan, in 2005 and 2017, respectively. After graduating from college, he was a Research and Development Officer with the National Chung-Shan Institute of Science and Technology and responsible for UAV management. His research forces on UAV control.